Chem Soc Rev

REVIEW ARTICLE

Ionic liquid-based green processes for energy production

Cite this: DOI: 10.1039/c3cs60409h

Suojiang Zhang,*[a] Jian Sun,[a] Xiaochun Zhang,[a] Jiayu Xin,[a] Qingqing Miao[a] and Jianji Wang[b]

Received 12th November 2013

DOI: 10.1039/c3cs60409h

www.rsc.org/csr

To mitigate the growing pressure on resource depletion and environment degradation, the development of green processes for the production of renewable energy is highly required. As a class of novel and promising media, ionic liquids (ILs) have shown infusive potential applications in energy production. Aiming to offer a critical overview regarding the new challenges and opportunities of ILs for developing green processes of renewable energy, this article emphasises the role of ILs as catalysts, solvents, or electrolytes in three broadly interesting energy production processes from renewable resources, such as CO_2 conversion to fuels and fuel additives, biomass pretreatment and conversion to biofuels, as well as solar energy and energy storage. It is expected that this article will stimulate a generation of new ideas and new technologies in IL-based renewable energy production.

1. Introduction

Currently, the majority of the world's energy consumption is derived from fossil fuels. The worldwide increase in energy demands has resulted in a trend of using fossil fuels, which are becoming exhausted. Consequently, it would be highly desirable and strategic to develop alternative fuels from non-fossil fuel sources.[1]

Nowadays, there is an increasing social expectation to produce renewable energy *via* green processes.[2,3] As novel and promising media, ionic liquids (ILs) have a number of favorable advantages, such as near-zero vapor pressure, high thermal stability, wide electrochemical window, and tunable properties as regards polarity, hydrophobicity, and solvent miscibility behavior through appropriate modification of the cations and anions.[4–8] Due to the unique properties of ILs, they

[a] Beijing Key Laboratory of Ionic Liquids Clean Process, State Key Laboratory of Multiphase Complex System, Institute of Process Engineering, Chinese Academy of Sciences, Beijing 100190, P. R. China. E-mail: sjzhang@home.ipe.ac.cn; Fax: +86-10-82627080; Tel: +86-10-82627080

[b] School of Chemistry and Chemical Engineering, Key Laboratory of Green Chemical Media and Reactions, Ministry of Education, Henan Normal University, Xinxiang, Henan 453007, P. R. China

Suojiang Zhang

Suojiang Zhang is Professor & Director General of the Institute of Process Engineering (IPE), Chinese Academy of Sciences (CAS). He received his PhD degree from Zhejiang University in 1994. Prof. Zhang mainly engages in ionic liquids and green process research, including molecular design, large-scale preparation and clean processes of ionic liquids. Until now, a total of 180 SCI papers have been published in academic journals, four monographs have been written or edited, and more than 40 patents have been authorized. He won the Second Class Prize of the National Natural Science Award of China in 2010.

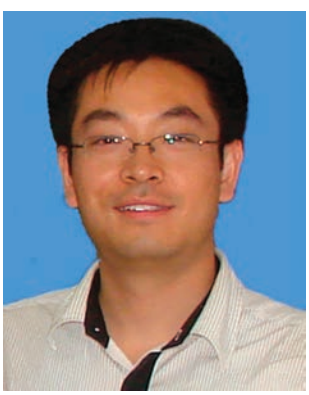

Jian Sun

Jian Sun received his PhD degree from the Institute of Process Engineering (IPE), Chinese Academy of Sciences (CAS) in 2009. Thereafter, he continued his academic career as an assistant professor at IPE, CAS, and was promoted to an associate professor in 2012. His research focuses on the design and application of ionic liquids in catalysis and organic synthesis, e.g. the development of energy-saving and clean processes utilizing CO_2 as C1 feedstock.

have been widely applied in many fields including catalysis, separation, photoelectric transformation, and material synthesis.[4,5,9–13] By searching the literature, it is found that there are plenty of papers linking the two keywords ILs and renewable energy, from which we witness the approaching of a new era of renewable energy with ILs.

The control of greenhouse gases (*e.g.* CO_2) that are concomitant with energy consumption is the most challenging environmental issue, and a cause of widespread concern in the world.[14] As an economical, safe, and renewable carbon source,[15] the conversion of CO_2 into energy not only contributes to alleviating global climate change, but also provides an opportunity in exploring new concepts and routes for energy to be recycled. However, due to the nature of inertia and the high oxidized state of carbon, the traditional conversion of CO_2 to fuels normally needs critical reaction conditions with heterogeneous catalysts. Due to the multiple functions of ILs in solubility enhancement, activation and electrochemical catalysis of CO_2, the unique performance of ILs in mild conversion of CO_2 to fuels gives birth to a new breakthrough.

Sustainable energy produced from renewable sources such as biomass,[16–20] and solar,[21,22] wind[23] and nuclear power,[24] has been predominately taken into account. Among them, biomass is an efficient and very attractive alternative, since biomass has ever been the primary energy historically, before the era of fossil fuels. The utilization of biomass generally includes two important steps, pretreatment and conversion. Traditional pretreatment usually uses toxic, corrosive and polluting agents such as H_2SO_4 and NaOH. ILs provide a new technology for the selective dissolution and extraction of cellulose or lignin. On the other hand, the conversion of cellulose or lignin to fuels is also a great challenge, due to the critical conditions required and low efficiency, thus more and more interest in IL-based conversion has been attracted in recent years.

Xiaochun Zhang

Xiaochun Zhang received her PhD degree from the Beijing University of Chemical Technology in 2009. Then she jointed the Institute of Process Engineering, Chinese Academy of Sciences as an assistant professor, and was promoted to an associate professor in 2012. Her research interests focus on studying the structure–property relationship of ionic liquids and the application of ionic liquids in dissolution and separation.

Jiayu Xin

Jiayu Xin received his PhD degree in Energy Science from Kyoto University, Japan in 2009. After graduation, he started to work as an assistant at the Institute of Process Engineering, Chinese Academy of Sciences. He is currently an associate professor and his current research interests include bio-energy, supercritical fluids and ionic liquid catalysis.

Qingqing Miao

Born in Hebei, China, Qingqing Miao received her PhD degree from Dalian University of Technology in 2011. She then started working as an assistant professor at the Institute of Process Engineering, Chinese Academy of Sciences in 2012. Her current research is focused on ionic liquids with greener synthetic methods, novel nanomaterials and their applications in high-performance solar cells, as well as new types of hybrid photovoltaic devices.

Jianji Wang

Dr Jianji Wang was educated in Chemistry at Henan Normal University (HNU, China), and received his MSc at Wuhan University (China), and PhD at Yokohama National University (Japan). He worked as a research fellow at University College London (1987–1989) and the University of Surrey (1992–1993). He became a professor of physical Chemistry at HNU in 1994. His current research interests are centered in the structure–property relationship of ionic liquids and their applications in green separation and biomass processing. He has authored around 200 scientific publications in peer-reviewed journals, and serves as an editorial board member of the Journal of Chemical Thermodynamics.

Solar energy is one of the most promising sustainable energies for the future.[25,26] The fundamental utilizations of solar energy are photoelectric, photothermal, photochemical and photobiological conversion. As the direct way to utilize solar energy, photoelectric chemical processes promise to offer a clean solution to the energy crisis. Electrolytes are one of the key components of photoelectric devices. However, traditional electrolytes have serious problems, for example, the volatility and instability troubles inherently related to the use of organic solvents. Recently, there have been lots of reports regarding the use of ILs in electrolytes to improve the efficiency and stability of photoelectric devices, which is becoming a hot and prospective research topic. Meanwhile, energy storage is being intensively developed due renewable energy sources such as solar and wind being discontinuous. ILs can play important roles in this aspect, because of their higher conductivity and wider electrochemical window compared to conventional solvents.

Following the above discussions, herein we aim to outline and review the research progress in the use of ILs in the three aspects:

(i) Chemical and electrochemical conversion of carbon dioxide to fuels and fuel additives, such as carbon monoxide, formic acid, alcohols, and cyclic/alkyl carbonates.

(ii) Pretreatment of biomass and thereafter the conversion to biofuels and chemicals such as bioalcohol, biogasoline, and 5-hydroxymethylfurfural (5-HMF).

(iii) IL-based electrolytes in the applications of solar energy and energy storage, such as solar cells, lithium-ion batteries, lithium–air batteries, supercapacitors and vanadium redox flow batteries.

This article intends to provide a reference and a new visual angle regarding the role of ILs in renewable energy production, not to provide a comprehensive summary by covering every related published reference.

2. CO_2 conversion to fuels and fuel additives

As the major greenhouse gas contributing to global warming, the average atmospheric concentration of CO_2 has increased from approximately 270 to 385 ppm during the last 200 years, with the fast development of industry and human society.[27] Until now, although many approaches have been tested aiming at the utilization of CO_2 to afford value-added chemicals, only a few have been commercialized including urea, methanol, cyclic carbonate and polycarbonate.[28,29] Recently, ILs have brought a new potential breakthrough for the conversion of CO_2 to fuels and/or fuel additives. Some typical routes are summarized in Fig. 1.

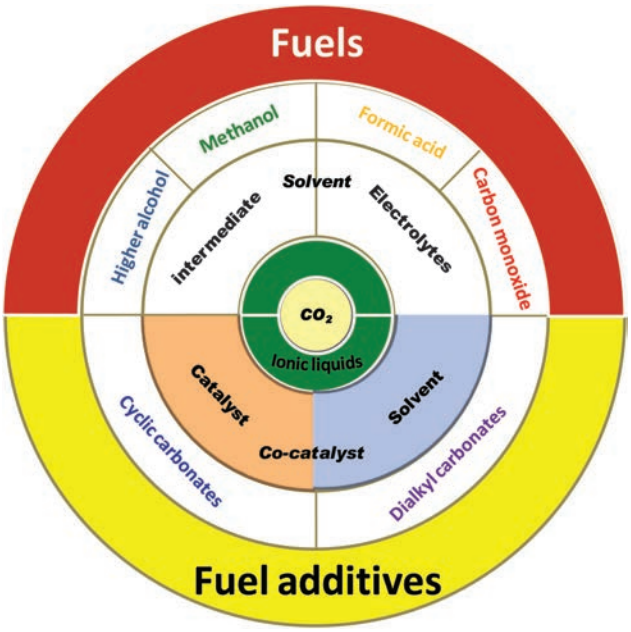

Fig. 1 Typical routes for the conversion of CO_2 to fuels and fuel additives with ILs.

2.1 Conversion of CO_2 to fuels

2.1.1 Carbon monoxide. The synthesis of carbon monoxide (CO) *via* CO_2 reduction is regarded as one important technology for the utilization of CO_2, because CO can be further transformed into many products, for example, the synthesis of oil by the Fischer–Tropsch process. In general, the corresponding reduction can be realized by three approaches: the reverse water gas shift reaction, electrochemical reactions and photochemical reactions. Developing an efficient process that can be performed under mild conditions is highly desired.

Chemical reduction. The reverse water gas shift reaction is a key reaction in the catalytic hydrogenation of CO_2 to produce liquid fuels. From a thermodynamic viewpoint, the reaction is endothermic with an enthalpy of ΔH_{298K} = 41.2 kJ mol^{-1} (eqn (1)), and thus high temperature would facilitate the formation of CO. Although various effective metal (Cu, Zn, Fe, *etc.*)-based heterogeneous catalysts are well developed for this reaction,[29] the drawback is that the operation is performed under very high temperatures, which results in high energy consumption and high running costs.

$$CO_2 + H_2 \leftrightarrow CO + H_2O,\ \Delta H_{298K} = 41.2\ \text{kJ mol}^{-1} \quad (1)$$

Nowadays, there is strong demand to develop new processes with innovative catalysts. There is some work exploring the utilization of ILs as catalysts in the reverse water gas shift reaction. For example, Tominaga and co-workers[30] proposed a new catalytic system composed of an ionic Ru cluster in the presence of bis(triphenylphosphine)imminium chloride ([PPN]Cl), realizing a low temperature condition of 160 °C compared to the traditional temperature of 300 °C.[31–34] The proposed mechanism is dehydrogenation of the hydride cluster, followed by coordination of CO_2 and electrophilic attack of a proton on its oxygen atom in the presence of chloride anions (Fig. 2).[30] During the process, the halide anions in the IL play a

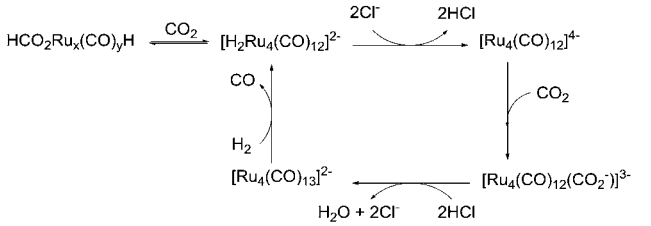

Fig. 2 A possible mechanism of the reverse water gas shift reaction catalyzed by Ru cluster anions/[PPN]Cl. Reprinted with permission from ref. 30.

role in deprotonating the Ru–H complexes, which is considered to be the rate determining step.[30]

Electrochemical reduction. Electrochemical reduction of CO_2 to fuels could also be a viable pathway for CO_2 remediation. The excellent electrochemical properties of ILs make them suitable electrolytes. Zhao *et al.* reported successful electrolysis in [BMIM][PF_6] from supercritical CO_2 ($scCO_2$) and water to produce CO and H_2 with a small amount of the byproduct formic acid.[35] The Faradic efficiency (FE) of CO increased obviously with increasing the pressure of CO_2, but the situation was contrary to H_2.[35] After the electrolysis, the products were extracted with $scCO_2$ and the IL was left in the electrolysis cell, which could be reused.

Bockris and co-workers proposed that the high overpotential for the conversion of CO_2 is the formation of a "CO_2^-" intermediate in the first step, and the equilibrium potential for CO_2^- formation is very negative in water and in most common solvents.[36,37] As a result, running the cathode as very negative (*i.e.*, at a high overpotential) is required for the reaction to occur, which is very energy-inefficient. Therefore, lowering the overpotential for the electrochemical process to CO is one of the grand challenges. Surprisingly, Rosen *et al.* made a breakthrough to overcome the high overpotential by using IL-mediated selective conversion of CO_2 to CO.[38,39] The overpotential could be reduced from about 1 volt to below 0.2 volts when 1-ethyl-3-methyl imidazolium tetrafluoroborate ([EMIM][BF_4]) was added into the reaction system (Fig. 3).[38] The IL electrolyte could lower the energy of the CO_2^- intermediate, most likely by complexation between CO_2 and $[BF_4]^-$, and thereby lower the initial reduction barrier.[38] Under the optimal conditions, the system could produce CO and last for at least 7 hours on a silver cathode at Faradaic efficiencies of above 96%, which were much higher than the Faradaic efficiency in the absence of IL (~80%). Using an inactive platinum cathode, the sum frequency generation (SFG) spectra results indicated two effects of [EMIM][BF_4] on the reaction: one was that it suppresses hydrogen formation and enhances CO_2 conversion, and the second was that it forms a complex such as CO_2–EMIM, which converts to adsorbed CO at a cathodic potential of −0.25 volts with respect to a standard hydrogen electrode.[39]

Thereafter, Rosen *et al.* found that the addition of water to [EMIM][BF_4] could enhance the efficiency of CO_2 conversion to

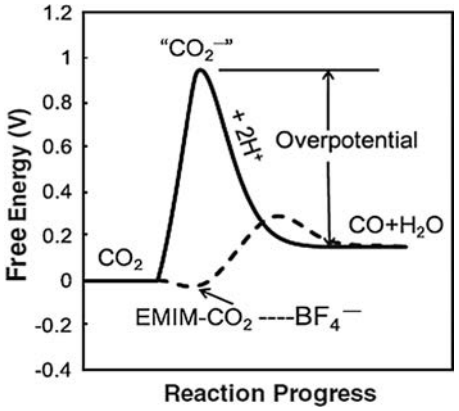

Fig. 3 A schematic comparison of the free energy for the electrochemical reduction of CO_2 in water or acetonitrile (solid line) or [EMIM][BF_4] (dashed line). Reprinted with permission from ref. 38.

CO on silver, which might be due to the lower overpotential for CO_2 conversion by water.[40] The corresponding result also showed that the [EMIM] cation could inhibit the H_2 evolution expected upon water addition, even at high water concentrations, that is [EMIM][BF_4] suppresses water electrolysis.[40]

Photoredox catalysis. Recently, Lin *et al.* reported the capture and activation of CO_2 by ILs coupled with photoredox catalysis to synthesize CO.[41] The structures of the cations and anions of the imidazolium ILs had considerable effects on the activation and reduction of CO_2 (Fig. 4). MeCN solvent with the addition of [TFSI] anions showed a significant promotional effect in the photocatalytic reaction. It was also found that the [EMIM][BF_4]/H_2O ratio showed a maximum value of CO_2 reduction efficiency at around 75%.[41]

2.1.2 Formic acid. Formic acid (FA) is a chemical of importance with numerous applications, including in fuel cells, and is industrially produced by employing CO as a raw material.[42] As an alternative method, a convenient FA production *via* CO_2

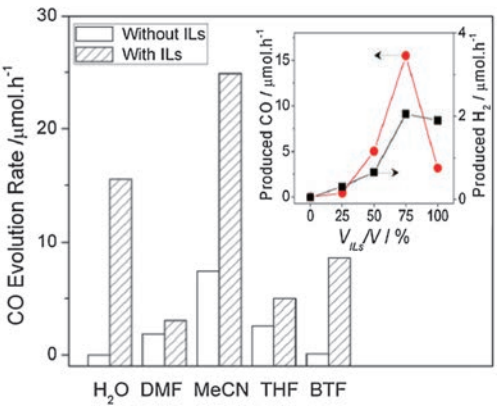

Fig. 4 The promotional effect of ILs on CO_2 photocatalytic reduction in various solvents. (DMF: *N*,*N*-dimethylformamide; MeCN: acetonitrile; THF: tetrahydrofuran; BTF: benzenyltrifluoride). The inset is the effect of [EMIM][BF_4]/H_2O ratio on the photocatalytic reduction of CO_2. Reprinted with permission from ref. 41.

hydrogenation is advantageous and deserves exploration, not only because CO_2 is abundant and inexpensive (eqn (2)),[43] but also because it would complete the long desired chemical loop for hydrogen storage using CO_2.[44–47] Furthermore, as an experimental way to store electricity, FA can also be produced from sunlight.[48–50] However, it has been indicated that the hydrogenation of CO_2 to formic acid is thermodynamically unfavorable (ΔG_{298} = 32.9 kJ mol^{-1}) unless a base is present, because the proton transfer to the base drives the reaction.[51] In addition, there is also an equilibrium for the reversible decomposition of FA into CO_2 and H_2 (eqn (2)). Accordingly, the existing methods intended for FA formation *via* CO_2 hydrogenation were proposed to use nitrogenous bases in polar solvents.[51] As a result, one equivalent of strong acid is needed to recover the FA from its formate salt, which results in complexity and pollution in the case of using a volatile base. Therefore, the development of new processes for the production of FA is highly required.

$$CO_2 + H_2 \leftrightarrow HCOOH \quad (2)$$

Recently, Zhang and co-workers developed a process for the synthesis of FA from CO_2 and H_2 using an amine-functionalized basic IL, which contains one or two tertiary amino groups on the cation as a promoter.[52,53] In a typical experimental procedure outlined in Fig. 5, after separation of the heterogeneous catalyst by filtration, the solution undergoes evaporation and distillation, respectively, to afford the product. The basic IL employed plays a role in the formation of a FA–IL salt *via* neutralization during the reaction and could be recycled with the aid of N_2 at 130 °C. The results also indicated that the addition of water could increase the rate of reaction, which is possibly due to its influence on the viscosity of the IL and on the formation of an intermediate.[53] Compared to the IL with a tertiary amino group on the cation,[52] an additional tertiary amino group on the cation of the IL facilitates two moles of FA per mole of the IL in one reaction cycle.

Yasaka *et al.* reported that the solvent effect on FA synthesis from H_2 and CO_2 could be understood by comparing the equilibrium constants in various chemical environments.[54] The different equilibrium constants in the IL, water and a vacuum revealed that the Coulombic solvation power of the IL 1,3-dipropyl-2-methylimidazolium formate ([PPMIM][HCOO]) played a key role in shifting the reaction equilibrium to the FA side.[54] In addition, the free energy diagram comparisons for FA production and separation in water and the IL are described in Fig. 6. Fig. 6a shows that the addition of a base in water results in larger solvation stabilization (black arrows) of the product side (HCOOH) than the reactant side (H_2 + CO_2), so the production process is energetically favored (the orange bold arrow with the circle means a useful level) in basic conditions.[54] However, FA must be recovered from the resultant formate salt by treating with a strong acid (*e.g.*, sulfuric acid), which would result in a large energy input requirement (the red bold arrow with the cross means not a useful level) for the separation process.[54] From environmental and economic viewpoints, the treatment process is not advantageous in industrial applications. If [PPMIM][HCOO] IL was used substituting for the traditional base, the HCOOH formation equilibrium could still be shifted effectively (orange bold arrow with the circle) but with little chemical waste and energy input (red bold arrow with the double circles, which means the most useful level) (Fig. 6b).

Recently, Wesselbaum and co-authors investigated the continuous-flow hydrogenation of CO_2 to pure FA using an integrated $scCO_2$ process with immobilized catalyst and base (Fig. 7).[55] The continuous removal of product from the reactor could be realized by using $scCO_2$ as both the reactant and extractive phase, and the reaction equilibrium could shift to

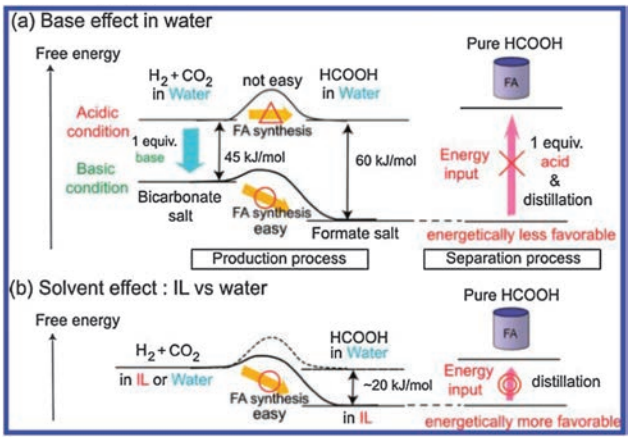

Fig. 6 Free energy diagram for formic acid (FA) production and separation in water and IL. (a) The base effect in water; (b) the solvent effect: IL *vs.* water. Reprinted with permission from ref. 54.

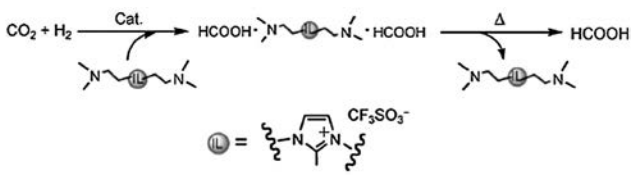

Fig. 5 Reaction scheme and separation process for the hydrogenation of CO_2 promoted by [DAMI][TfO]. Reprinted with permission from ref. 53.

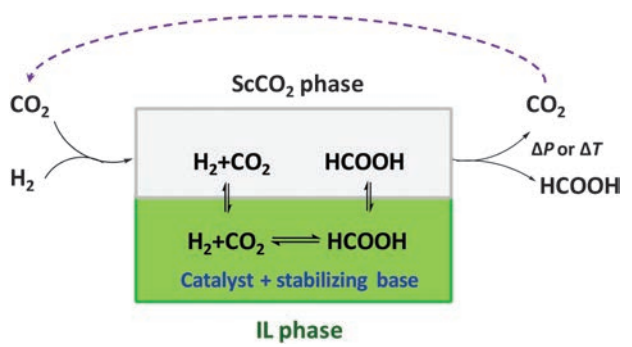

Fig. 7 The process for the direct continuous-flow hydrogenation of CO_2 to free formic acid with $scCO_2$ as the extractive mobile phase and an IL as the stationary phase containing the catalyst and the stabilizing base. Reprinted with permission from ref. 55.

readjust in the reactive phase. In addition, facile recovery of FA could be achieved by decompression of the CO_2 flow downstream.[56] Since the components in the IL phase are insoluble in $scCO_2$, FA without cross-contamination could be obtained.

2.1.3 Alcohols

Methanol. Methanol is an important chemical that finds applications in various industrial processes. Since it can be directly used as a fuel or as an additive to gasoline, and can also be used as a platform chemical for the synthesis of various fuels and chemicals (*e.g.* biodiesel), research on conversions into methanol has been a continuously attractive topic for a long time.[57–62] Generally, methanol can be produced from CO_2/CO and H_2 (eqn (3) and (4)). From a thermodynamic viewpoint, an increase in reaction pressure or a decrease in reaction temperature could favor the synthesis of methanol. On the other hand, from a kinetic viewpoint, enhanced reaction temperature (*e.g.* higher than 240 °C) facilitates CO_2 activation and the subsequent methanol formation rate.[29,63]

$$CO_2 + 3H_2 \rightarrow CH_3OH + H_2O \quad (3)$$

$$CO + 2H_2 \rightarrow CH_3OH \quad (4)$$

Since the first industrial production of methanol by BASF in 1923 from syngas in the presence of zinc and chromium catalysts at very critical reaction conditions (360–400 °C and 20–30 MPa), various metal-based catalysts have been developed aiming to enhance the productivity under mild reaction conditions, among which Cu remains the main active catalyst component, together with different modifiers (Zn, Zr, Ce, Al, *etc.*).[29] Recently, some tentative research has been reported on the conversion of CO_2 into methanol *via* an imidazolium ionic intermediate. As an example, using imidazolium N-heterocyclic carbene (NHC) catalysts and silanes as hydride donors, Riduan and co-workers developed the first metal-free catalytic conversion of CO_2 to produce methanol with over 90% yield under ambient conditions (Fig. 8).[57] An imidazolium carboxylate was formed from the activation of CO_2 by NHC, which was proposed to be more reactive towards silanes.[57] Compared to conventional transition-metal catalysts for CO_2 reduction with silanes, NHC presents tolerance to oxygen and superior efficiency.[57] Thereafter, in order to gain insight into the catalytic mechanism, Huang and co-workers conducted a further computational study with density functional theory.[64] By comparison of the two possible activation modes (Fig. 9), it was proposed that NHC prefers to activate the Si–H bonds of silanes (mode B) and push electron density to the H atoms of the Si–H bonds, favoring the transfer of a hydridic atom of the silane to the electrophilic C center of CO_2/formoxysilane/HCHO.[64]

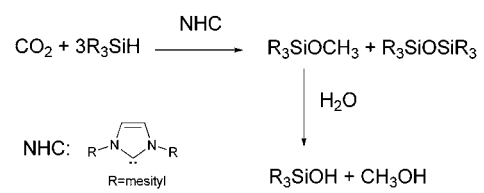

Fig. 8 Conversion of carbon dioxide into methanol with silanes over N-heterocyclic carbene catalysts. Reprinted with permission from ref. 57.

Higher alcohols. Higher alcohols are preferable to methanol from the viewpoint of safe transport and excellent compatibility with gasoline.[65] As an efficient route for producing alcohols, hydroformylation has become one of the most important processes in industry, however, the reaction is conventionally carried out using metal complex catalysts in volatile organic solvents with highly toxic CO as a reactant.[66] With the aim of using CO_2 as an alternative to CO, a new hydroformylation method catalyzed by homogeneous transition metal complexes using CO_2 as a reactant has been reported by Tominaga, in which ILs are introduced to replace organic solvents.[66] It was found that a mixed ionic liquid [BMIM][Cl + TFSI] system was successfully used as a reaction medium for Ru-catalyzed hydroformylation of 1-hexene with CO_2 in the absence of CO and any volatile organic solvents (Fig. 10). When the Cl^- anions were replaced with TFSI anions, the conversion of 1-hexene along with the yield of heptanol and hexane gradually increased. The yield of alcohol reached a maximum when the mol fraction of $TFSI^-$ was about 0.5, and decreased with further replacement. The yields and TONs are higher than those reported previously using conventional organic solvents (*e.g.* toluene and *N*-methyl-2-pyrrolidone).[66] After distillation, the reaction medium containing the Ru-catalyst could be successfully recycled.

2.2 Conversion of CO_2 to fuel additives

Efforts have been made to produce fuel additives from CO_2 without using a hydrogen source. Generally, this non-hydrogenation process results in carbonates and carbamates, among them carbonates including cyclic carbonates and dialkyl carbonates were found to be effective fuel additives.[67] As is well known, there are several previous review papers regarding this theme,[28,68–72] herein we briefly summarize the latest progresses on the synthesis of the above two typical carbonates.

2.2.1. Cyclic carbonates. Up until now, there have been numerous reports on IL catalytic conversion of CO_2 to cyclic carbonates such as ethylene carbonate and propylene carbonate, and this flourishing progress seems to go on. To the best of our knowledge, it could be generally summarized into two primary catalytic systems for the synthesis of cyclic carbonates related to ILs, one is Lewis acid/IL and the other is hydrogen bond donor/IL.

Lewis acid/IL process. Research on Lewis acid/IL processes has been dominant in the past twenty years. The presence of Lewis acids could remarkably enhance the activity of ILs due to their strongly synergetic catalysis role. Nowadays, although a variety of metallic based compounds have been tested for this reaction,[68–71] zinc salts are still the primary Lewis acid candidates because of their comparative low cost and high efficiency. As another matched component, the majority of ILs used in the literature are salts of quaternary ammonium, phosphonium, imidazolium and pyridinium cations with inorganic counter anions.[68–71] It is accepted that the ILs with cations of bulkier

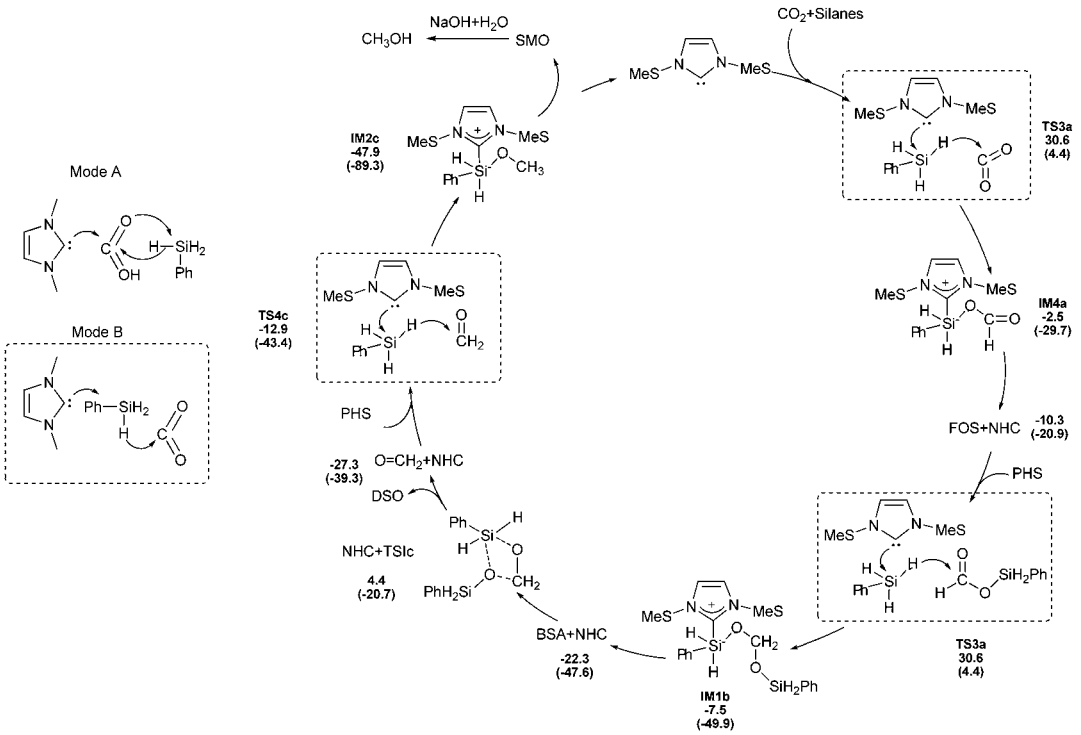

Fig. 9 Detailed mechanism of the whole catalytic cycle, and the values below the names of the stationary points are the free energies and entropies (kcal mol^{-1}) (in parentheses) relative to NHC$_{exp}$ + 3PHS + CO_2. Reprinted with permission from ref. 64. (SMO: silylmethoxide; FOS: formoxysilane; PHS: phenylsilane; BAS: bis(silyl)acetal; DSO: disiloxane; NHC$_{exp}$: 1,3-bis(2,4,6-trimethylphenyl) N-heterocyclic carbene).

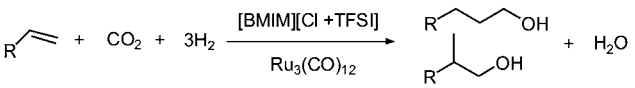

Fig. 10 Ru-catalyzed hydroformylation of 1-hexene with CO_2 in the presence of ILs. Reprinted with permission from ref. 66.

alkyl chain length and with more nucleophilic anions (*e.g.* Cl^-, Br^-, and I^-) have better reactivity. Without considering the details of the reaction path, a very brief mechanism can be summarized as shown in Fig. 11a according to our previous work,[73] and related reviews.[68,70–72] In a typical process, the synergistic effect of the binary catalyst for ring-opening of the epoxide results from the nucleophilicity of the highly reactive anions of the ILs and the electrophilicity of the Lewis acid as has been well discussed, and this is generally considered as the rate-controlling step.

Hydrogen bond donor/IL process. As another category, the hydrogen bond donor/IL catalysis process has attracted more attention in recent years, because this kind of system could exhibit better tolerance to water compared to Lewis acid/IL systems.[71] The presence of hydrogen bond donors (HBDs), chemicals containing hydroxyl groups, could contribute a positive role on the activity of ILs due to hydrogen bond interactions between the epoxide ring and the HBD, which accelerates the ring opening of the epoxide. The mechanism is different from that in Lewis acid/IL systems (Fig. 11b). In the case of R′═H (Fig. 11b), Zhang *et al.* reported that the presence of water could remarkably improve the activities of ILs, by which the turnover frequency of the reaction is about 4–5 times higher than that in the absence of water.[74] Based on the experimental results and the related DFT study,[74,75] it was proposed that the activation and ring-opening of the epoxides through hydrogen bonding were the key steps for making the catalytic process proceed smoothly.

IL process. The low catalytic activities of traditional ILs restrain their direct use for the synthesis of cyclic carbonates from CO_2, which is the main reason why binary IL systems have attracted much attention recently. However, from the viewpoint of operation in a real application, a simple and efficient catalyst is still needed. Inspired by the HBD synergistic catalysis role, hydrogen bonding functionalized ILs have been developed (Fig. 12) and exhibit much higher activities than expected compared to the unmodified ILs. A synergetic catalysis effect resulting from the –OH (Fig. 12a) or –COOH (Fig. 12b) group (as a HBD unit) and the Lewis basic anion of the IL (as a nucleophilic attacking site) was proposed to play an important role in accelerating the ring opening of the epoxide.[76–79]

2.2.2. Dialkyl carbonates (*e.g.* dimethyl carbonate). Dimethyl carbonate (DMC), which is a linear alkyl carbonate with low toxicity and biodegradability, is an important chemical for synthesis of many products such as polycarbonates instead of phosgene.[72,80,81] It is also an ideal additive to

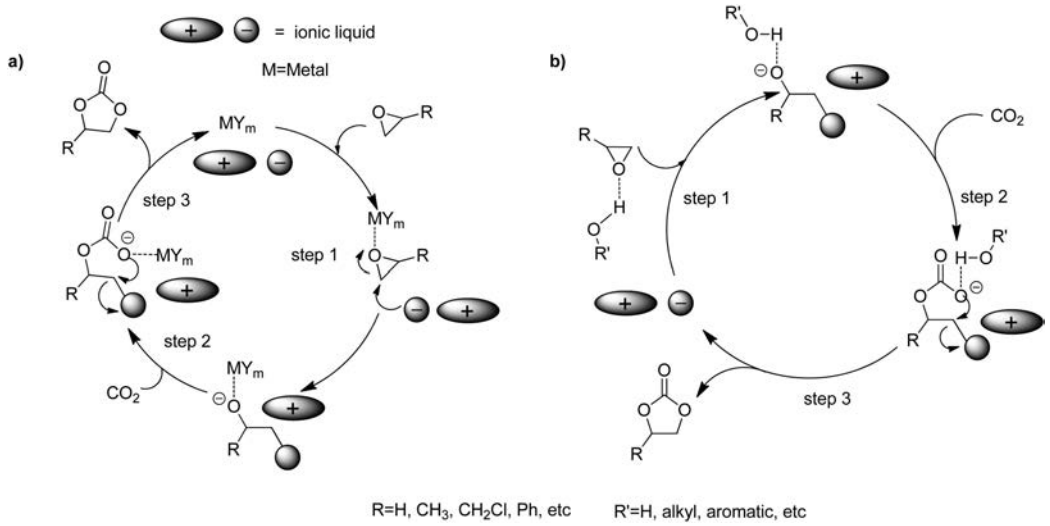

Fig. 11 Proposed mechanisms of Lewis acid/IL system (a) or HBD/IL system (b) catalyzed synthesis of cyclic carbonates.[71,73,74]

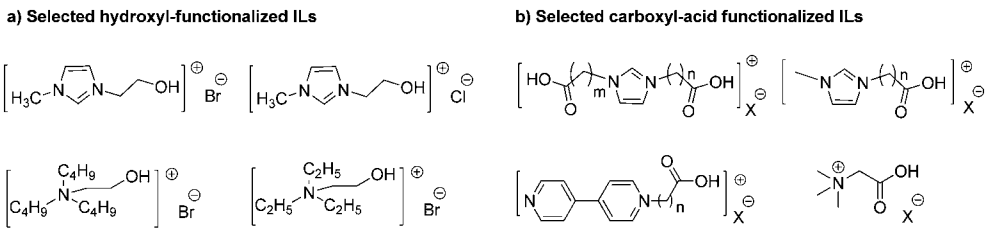

Fig. 12 Selected hydroxyl-functionalized and carboxyl-acid functionalized ILs. Reprinted with permission from ref. 76 and 77.

gasoline or fuel oil for transportation due to its good blending octane ($R + M/2 = 105$) and because it does not phase separate from oil.[72,80] Herein, we review two routes, catalytic processes and electrochemical processes, for the synthesis of DMC with ILs.

Catalytic process. Zhang and co-workers synthesized a series of $Ce_xZr_{1-x}O_2$ (x = 0.2, 0.3, 0.4, 0.5, 0.6, 0.8, 1.0) solid solutions with a bimodal pore structure, and investigated their catalytic performances for the selective production of DMC from CO_2 and CH_3OH (Fig. 13a) in the presence of 1-ethyl-3-methylimidazolium bromide ([EMIM]Br).[82] Water was *in situ* dehydrated by 1,1,1-trimethoxymethane (TMM) to overcome the thermodynamic limitations (Fig. 13b), by which the methanol conversion catalyzed by $Ce_xZr_{1-x}O_2$ was increased from 1.8 to 7.9%. By examining the methanol conversion, 50 wt% of TMM gave the maximum conversion of 10.4% at 12 MPa, 100 °C over 34 h, far above the equilibrium value without TMM. The results also showed that the catalytic activity was almost doubled when the ratio of [EMIM]Br to $Ce_{0.5}Zr_{0.5}O_2$ is 1/3 compared to that with the $Ce_{0.5}Zr_{0.5}O_2$ catalyst alone.

Du and co-workers developed a method for the synthesis of DMC *via* the [BMIM]Cl promoted carbonylation reaction of methanol and CO_2 over K_2CO_3/CH_3I under microwave irradiation (Fig. 14).[83] Based on the simulation, the authors proposed that the reaction medium ILs may play primary roles in regulating intermediate polarity and the dipole moment of the transition state, by which the selective absorption of

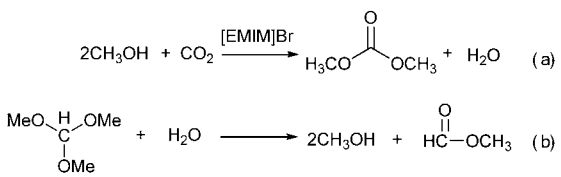

Fig. 13 Ionic liquid promoted synthesis of DMC from CO_2. Reprinted with permission from ref. 82.

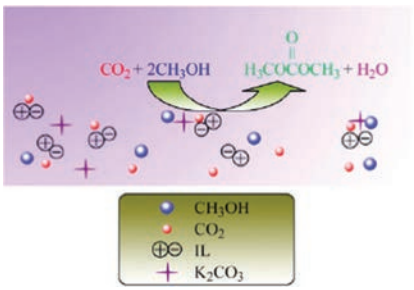

Fig. 14 Scheme of an IL promoted catalytic reaction for the synthesis of DMC. Reprinted with permission from ref. 83.

microwave energy and the solubility of CO_2 in the reaction system were increased.[83] As shown in Fig. 14, this increased the transportation of CO_2, and the number of reactive molecule collisions between CO_2 and CH_3OH, which happened around K_2CO_3 molecules, thus improving the catalytic activity.[83]

Chen and co-workers investigated the one-pot synthesis of DMC from propylene oxide, CO_2, and methanol (Fig. 15) catalyzed by 1-butyl-3-methylimidazolium tetrafluoroborate ([BMIM][BF_4])/$NaOCH_3$.[84] The amount of [BMIM][BF_4] had little effect on the conversion of propylene oxide, but significantly affected the selectivity of DMC, in which an insufficient (<0.6 mL) or an excessive amount (>0.6 mL) of [BMIM][BF_4] resulted in a relatively low yield of DMC.[84] Under the optimal reaction conditions (PO : CH_3OH = 25 mmol : 200 mmol, 4 MPa, 5 h, 150 °C, CH_3ONa 0.25 g, [BMIM][BF_4] 0.6 mL), a high yield (67.6%) of DMC was reached.

Electrochemical process. Dialkyl carbonate can also be electro-synthesized.[85–87] Zhang *et al.* established a new electrochemical procedure for the synthesis of dialkyl carbonates in a CO_2-saturated [BMIM][BF_4] solution with addition of an alkylating agent under mild conditions, P_{CO_2} = 1.0 atm, T = 55 °C, (Fig. 16).[85] The corresponding process avoided using organic solvents and supporting electrolytes. CO_2 reduction in IL was comparatively easier than that in organic solvents, which may be attributed to the formation of a CO_2^-–BMIM$^+$ ion-pairing.[85]

Wu and co-workers provided a procedure for the utilization of NHC, which is electrogenerated from [BMIM]X (X = $[BF_4]^-$, $[PF_6]^-$), for the synthesis of dialkyl carbonates under mild conditions with high conversion and excellent selectivity (Fig. 17).[86] NHC–CO_2 formation was supported by electrochemical analysis. The IL performed a dual role as a green solvent and a NHC precursor during the process, by which the use of organic solvents and the addition of supporting electrolytes is avoided.

As another example, electrocatalytic activation and conversion of methanol and CO_2 to DMC with graphite and platinum electrodes in a dialkylimidazolium IL–methanol system was conducted under ambient conditions.[87] Among the investigated ILs (Table 1), 1-benzyl-3-methylimidozolium chloride ([BzMIM]Cl) showed the best performance for electrochemical synthesis of DMC with 3.8% yield and 51.8% selectivity to DMC. Although [BMIM]Cl and [BMIM][OH] presented almost the same activity (3.7% and 3.1%, respectively) for synthesis of DMC, the selectivity to DMC is very low (12.9% and 42.5%, respectively).[87]

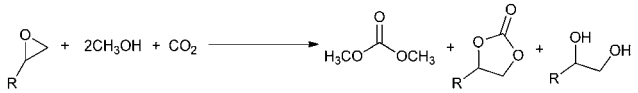

Fig. 15 IL promoted synthesis of DMC from CO_2, methanol and epoxide.

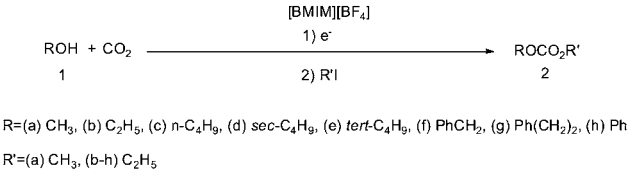

Fig. 16 Electro-synthesis of dialkyl carbonates from alcohol and CO_2 in [BMIM][BF_4]. Reprinted with permission from ref. 85.

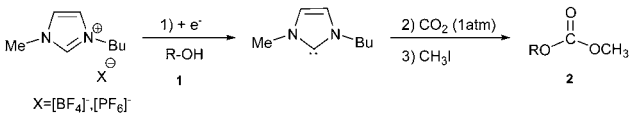

Fig. 17 Synthesis of dialkyl carbonates from CO_2 and alcohols *via* electrogenerated NHC. Reprinted with permission from ref. 86.

Table 1 Synthesis of DMC in different ILs[a]

Entry	ILs	Y (%)	S_{DMC} (%)	S_{DMM} (%)
1	[BzMIM]Cl	3.8	51.8	41.9
2	[BMIM]Cl	3.7	12.9	9.3
3	[BMIM][OH]	3.1	42.5	38.5
4	[BMIM]Br	2.1	39.7	47.0
5	[BMIM][BF_4]	0.3	15.5	77.7
6	[EMIM][BF_4]	1.3	37.6	39.2
7	[EMIM]Br	0.6	24.3	49.7

[a] Y: yield; S: selectivity; DMM: dimethoxymethane.

3. Biomass conversion to biofuels

Lignocellulosic materials, such as agricultural residues (corn stover and wheat straw), waste paper, wood wastes, and energy crops have been recognized as important resources for producing fuels. As shown in Fig. 18, biomass is composed of

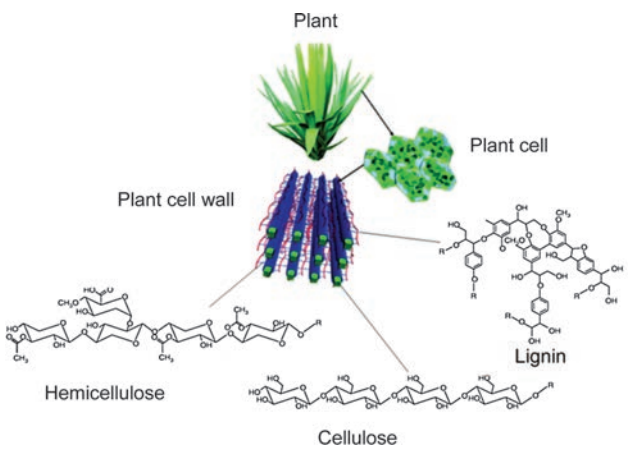

Fig. 18 Composition of biomass, modified from ref. 88. Reprinted with permission from ref. 88.

cellulose, hemicellulose and lignin. Among these components, cellulose and hemicellulose make up 60–90 wt% of biomass.[88]

Cellulose is a crystalline material that consists of a linear polysaccharide of D-glucopyranose monomers with β-1,4 linkages, while hemicellulose is a polymer of five-carbon sugars (xylose and arabinose) and six-carbon sugars (galactose, glucose, and mannose). Lignin, the other major component of biomass, is a highly branched and substituted mononuclear aromatic polymer found in the cell walls of woody biomass. Biomass can be converted into liquid fuels by three routes as shown in Fig. 19.

Since the report of ILs as solvents for the dissolution of cellulose in 2002,[89] a lot of work has appeared in this field, which demonstrates the huge potential of ILs for dissolution of biomass and the conversion of biomass into biofuels and chemicals.

3.1 Dissolution of biomass

This section aims to summarize the current state of the research on the dissolution of biomass, including cellulose, lignin and natural lignocellulose with ILs. The dissolution of hemicellulose has not be extensively reported, thus it was not including in this paper.

3.1.1 Dissolution of cellulose

Various ILs for dissolving cellulose. Owing to its extensive network of inter- and intra-molecular hydrogen bonds and van der Waals interactions between cellulose fibers,[90] it is very difficult to dissolve or melt cellulose in common solvents,[91] resulting in barriers to its further utilization. Therefore, the development of effective solvents to dissolve cellulose is an important prerequisite for the use of cellulose.

As early as in 1934, Graenacher discovered that molten *N*-ethylpyridinium chloride could be used to dissolve cellulose in the presence of nitrogen-containing bases.[92] However, this finding did not attract enough attention at that time due to the limited knowledge of the structures and interactions of cellulose and the relatively high melting point (118 °C) of *N*-ethylpyridinium chloride.

In 2002, Swatloski and co-workers found that the IL 1-butyl-3-methylimidazolium chloride ([BMIM]Cl), showed an excellent performance for dissolving cellulose, with as high as 25% of the cellulose being dissolved in the IL with the aid of heating with microwaves, and 10% without microwaves.[89] Since then, ILs have received worldwide attention and are regarded as promising solvents in the dissolution of cellulose under mild conditions.[93,94] Zhang *et al.*[95,96] synthesized a novel ionic liquid, 1-allyl-3-methylimidazolium chloride ([AMIM]Cl), for readily dissolving nearly 30% of cellulose below 100 °C. Compared with [BMIM]Cl, [AMIM]Cl has a higher capability for the dissolution of cellulose, a relatively lower melting point (17 °C) and a higher thermal stability.

Subsequently, Ohno *et al.*[97–99] found that the ILs *N*,*N*′-dialkylimidazolium formates ([RR′MIM][HCOO]) and 1-methyl-3-ethylimidazole methylphosphate ([EMIM][(MeO)(R)PO_2]) with strong hydrogen bond acceptability, can dissolve cellulose, silk, carbohydrates and other biomacromolecules. Wherein, [AMIM][HCOO] and [EMIM][(MeO)(R)PO_2] exhibited relatively low viscosities, as well as low temperature and good ability to dissolve cellulose. In 2008, Zhao *et al.*[100] synthesized several new enzyme-compatible ILs that can not only dissolve cellulose but can maintain the activity of the enzyme. Imidazolium acetate, containing an alkyloxyalkyl chain in the cation ([Me(OEt)$_n$-EIM]), can alleviate the enzyme denaturalization caused by conventional halogen anions to some extent. In 2009, Amarasekara *et al.*[101] synthesized Brönsted acidic ILs, 1-(1-propylsulfonic)-3-methylimidazolium chloride and 1-(1-butylsulfonic)-3-methylimidazolium chloride, for hydrolysis and decomposition of Sigmacell cellulose (DP = 450), and the results showed that the ILs are effective in dissolution of cellulose at room temperature and atmospheric pressure without any pretreatment. In addition, these ILs were also found to hydrolyze cellulose to give reducing sugars at elevated reaction temperatures. In 2010, Xu *et al.*[102] synthesized a series of ILs by coupling 1-butyl-3-methyl-imidazolium cations [BMIM] with Brønsted basic anions including $[OAc]^-$, $[HSCH_2COO]^-$, $[HCOO]^-$, $[(C_6H_5)COO]^-$, $[H_2NCH_2COO]^-$, $[HOCH_2COO]^-$, $[CH_3CHOHCOO]^-$ and $[N(CN)_2]^-$. It was found that the solubility of cellulose increases almost linearly with an increase in the hydrogen bond accepting ability of the anions in the ILs. Until now, dozens of ILs have been reported for the dissolution of cellulose,[80,93–95,103] several of the main ones used are listed in Fig. 20. Among these, [BMIM]Cl, [AMIM]Cl and [EMIM][OAc] are most often used in studies.

Moreover, it is found that the solubility of cellulose can be significantly increased by adding lithium salts (LiCl, LiBr, LiOAc, $LiNO_3$, or $LiClO_4$) into ILs, which is because the interaction of Li^+ with the hydroxyl oxygen of cellulose disrupts the intermolecular hydrogen bonds in cellulose. Also, it is found that co-solvents, such as DMI, DMF, DMSO *etc.*, can influence the solubility of cellulose in ILs.[104–106] In addition, high-intensity energy means, for example ultrasound and microwaves, can effectively promote the dissolution of cellulose in ILs.[89,107,108]

Mechanism of cellulose dissolution with ILs. With respect of the mechanism of cellulose dissolution in ILs, it is proposed that the formation of hydrogen bonds between the ILs and the cellulose hydroxyl groups is the key factor in breaking the inter- and intra-molecular hydrogen bonds of cellulose. The stronger the hydrogen bond accepting ability of the ions, the greater the

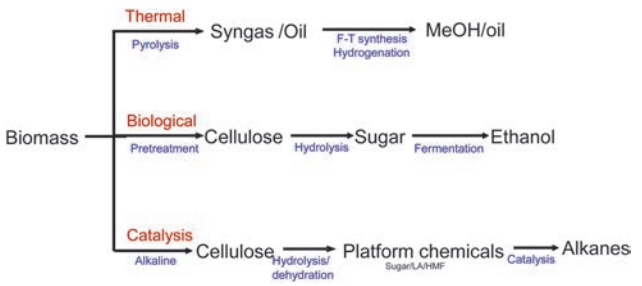

Fig. 19 Three routes for the conversion of biomass to biofuels.

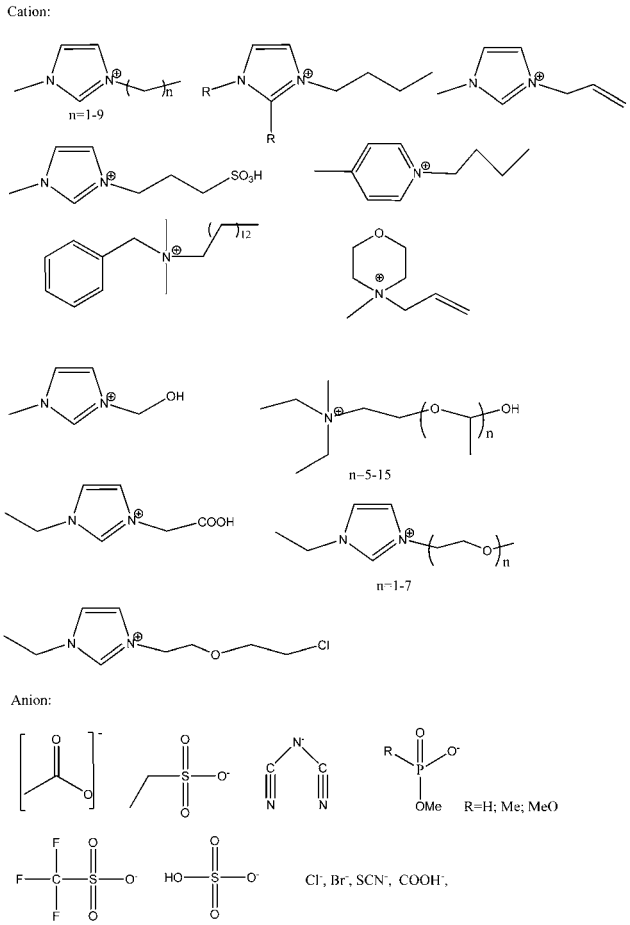

Fig. 20 Several of the mainly used ILs for cellulose dissolution.

capacity to dissolve cellulose.[98,99,109–111] However, the respective roles of the anions and cations is not yet clearly understood, particularly the role of cations in the dissolution process. Regarding [BMIM]Cl, Swatloski *et al.* proposed that the strong hydrogen bonds between Cl anions and the hydroxyl groups of cellulose are the decisive factor for the dissolution,[89] which was confirmed by ^{13}C and $^{35/37}Cl$ NMR relaxation measurements[112,113] and molecular dynamics studies.[114] A more general viewpoint is that the role of cations can't be ignored by investigating various types of ILs.[115–118] For example, the ability of ILs to dissolve cellulose changes and is even lost when the imidazolium and pyridinium cations are replaced by other types of cations, while keeping the same anion.[119] Even if the C2–H of the imidazolium ring is substituted by a methyl group, the solubility of cellulose substantially decreases.[120] Such a viewpoint was further proven by simulation studies. For example, Youngs *et al.*[121] revealed weak hydrogen bonding and van der Waals interactions between glucose and the [DMIM] cation.

Zhang *et al.*[122–124] systematically studied the effects of anions and cations on the dissolution of cellulose by molecular dynamics simulations and proposed that the synergistic interactions between the anions and cations with the cellulose hydroxyl groups lead to the dissolution of cellulose in ILs. To be good candidates for cellulose dissolution, the anions of ILs

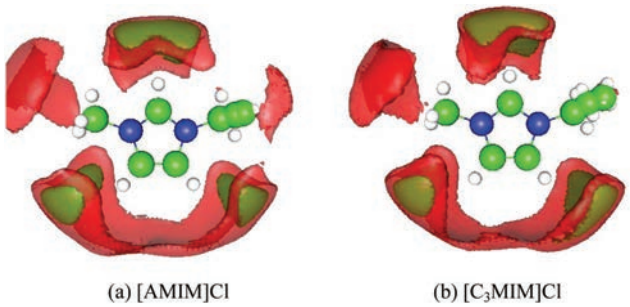

Fig. 21 Spatial distribution functions for pure (a) [AMIM][Cl] and (b) [C_3MIM][Cl]. Reprinted with permission from ref. 122.

should have the following features: (1) high electron density to form hydrogen bonds with cellulose; (2) short alkyl chains to decrease the steric hindrance effect; (3) no electron-withdrawing groups.[124] Zhang *et al.*[122] further studied the effect of cations on the dissolution of cellulose by investigating mixtures of cellulose with a series of imidazolium-based chloride ILs, including 1-alkyl-3- methyl imidazolium ([C_nMIM]Cl (n = 2, 3, 4, 6, 8, 10)), 1-butyl-3-methyl pyridinium chloride ([C_4MPy]Cl) and 1-allyl-3-methyl imidazolium chloride ([AMIM]Cl), from which, it was found that [C_4MPy] is better than [C_4MIM]. In addition, the presence of electron-withdrawing groups in the alkyl chain of the cations enhances the interaction between the cations and cellulose due to the increase of electronegativity and thus enhances the solubility of cellulose. As shown in Fig. 21, the biggest difference in the spatial distribution functions of [AMIM]Cl and [C_3MIM]Cl is the distribution of the anion around the long alkyl chain. In the first solvation shell, some anions are distributed around the alkyl chain of $[AMIM]^+$ rather than $[C_3MIM]^+$. This implies that the addition of an allyl group increases the electronegativity of the cation.

Similar work performed by other researchers also proved that both IL cations and anions are important for efficient dissolution of cellulose. The anions form hydrogen bonding interactions with cellulose, while the cations interact with cellulose by charge delocalization.[96,98,125–130]

Recently, the mechanism of the effect of co-solvents on cellulose dissolution was investigated by Zhang *et al.*[123] They found that the effect of a co-solvent on cellulose dissolution is indirectly achieved by influencing hydrogen bond interactions between the anion and cellulose. The strong preferential solvation of $[OAc]^-$ by protic solvents (such as CH_3OH and H_2O) can compete with the hydrogen bond interaction of cellulose–[OAc] in the dissolution process, resulting in decreased cellulose solubility. Aprotic solvents (such as DMSO and DMF) can partially break down the ionic association of [BMIM][OAc] by solvation of the cations and anions and then improve the dissolution of cellulose. Furthermore, the effect of the DMSO-to-[C_4MIM][OAc] molar ration on cellulose solubility was investigated, and a possible dissolution mechanism was proposed, as shown in Fig. 22.

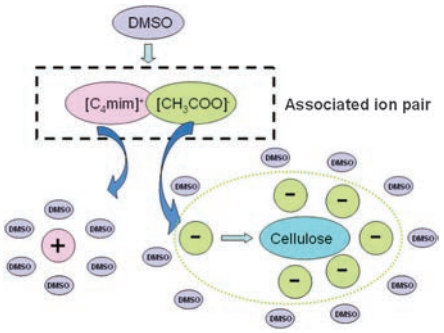

Fig. 22 The schematic illustration for the dissolution mechanism of cellulose in [C_4MIM][OAc]/DMSO with the molar ratio corresponding to the strongest interaction between the IL and cellulose. Reprinted with permission from ref. 123.

3.1.2 Dissolution of lignin. Lignin is the third most abundant biopolymer on the earth,[131–135] and the only natural non-petroleum resource that can provide aromatic compounds.[136] Traditional methods for the separation of lignin are decating of lignocelluloses with inorganic acids and alkalis, or extraction with organic solvents.[137–139] There are shortcomings for both the economic and environmental aspects of these methods. Based on previous reports,[140–142] the utilization of ILs for the dissolution of lignin is a promising alternative to traditional methods.

The dissolution of lignin in ILs has been studied by many researchers. Fu *et al.*[143] used six kinds of ILs to dissolve lignin extracted from straw, and found that all six ILs can dissolve lignin (≧10 g per 100 g), among which [EMIM][OAc] showed the most excellent performance with a 30% lignin–IL solution at 90 °C. Pu *et al.*[133] demonstrated that for the $[BMIM]^+$ based ILs, the order of lignin solubility for the varying anions is: $[MeSO_4]^-$ > Cl^-, Br^- ≫ $[PF_6]^-$, which indicates that the solubility of lignin is principally influenced by the nature of the anions. Similarly, Lee *et al.*[144] found that [MMIM][$MeSO_4$] and [BMIM][CF_3SO_3] are the most effective solvents for dissolving Kraft lignin, the lignin solubilities of both solvents are >500 g kg^{-1} (lignin–IL), followed by [EMIM][OAc] and [AMIM]Cl, the lignin solubilities in which are >300 g kg^{-1}. [BMIM]Cl and [BzMIM]Cl show a very limited ability to dissolve lignin, although [BMIM]Cl is an effective solvent for cellulose. Moreover, [BMIM][BF_4] and [BMIM][PF_6] are unsuitable for dissolution of lignin, which is similar to the result reported by Pu *et al.*[133]

It can be summarized that the main force for the lignin dissolution process is hydrogen bonding, while secondary and insignificant contributions come from the electrostatic forces and van der Waals interactions, respectively. In addition, the anion plays the major role in the formation of hydrogen bonding during the dissolution process; the most promising anions are $[OAc]^-$, $[HCOO]^-$ and Cl^-, while the larger, non-

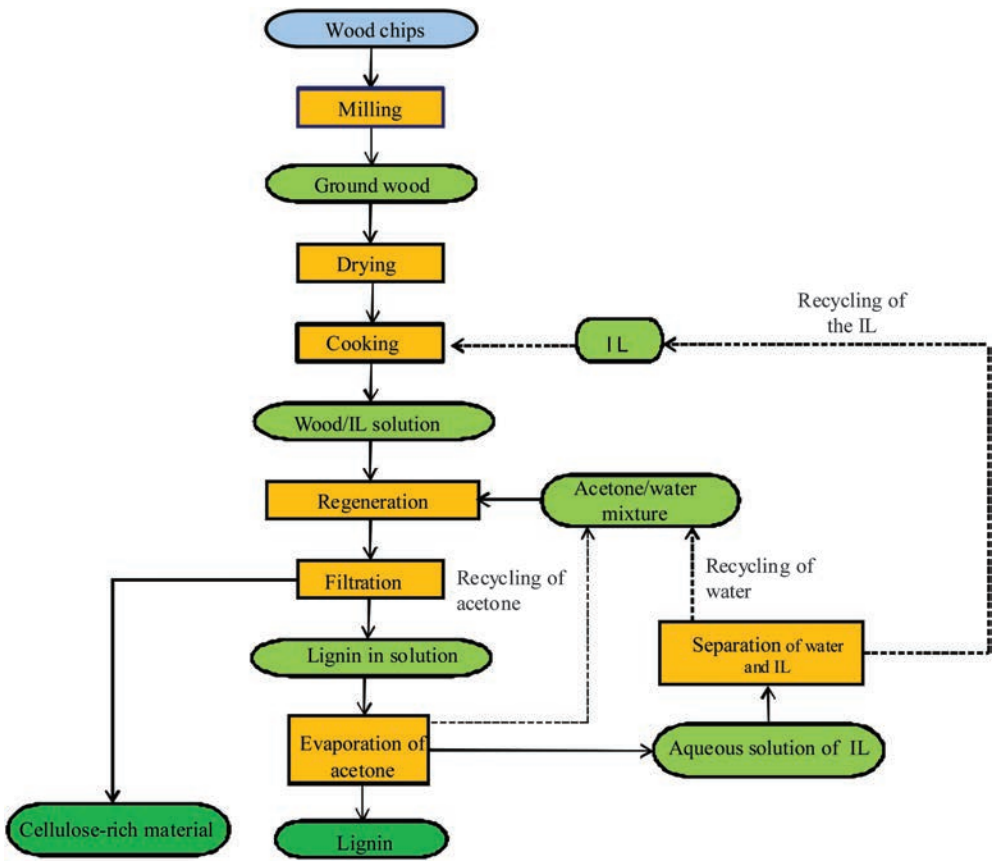

Fig. 23 The general procedure for the dissolution and regeneration of wood in IL. Reprinted with permission from ref. 149.

coordinating anions such as $[BF_4]^-$, $[PF_6]^-$ and Br^- are inefficient, which was further confirmed by Casas *et al.*[141] *via* COSMO-RS simulations.

3.1.3 Dissolution of natural lignocellulose. Due to the intricate, complex and rigid structure of lignocellulose,[145,146] generally, dissolution and separation of natural lignocellulose are performed by thermochemical and/or physical methods.[147] However, the conventional methods have limitations such as insufficient selectivity and partial degradation of the products. Recently, a lot of effort has been focused on understanding the pathways to improve the selective separation of lignocellulose to accomplish feasible and sustainable processes based on ILs.

Argyropoulos *et al.*[148] reported the complete dissolution of 8 wt% of a dried wood sample in [BMIM][Cl] and [AMIM][Cl] at temperatures from 80 to 130 °C. A similar result was reported with [EMIM][OAc] by Sun *et al.*[149] Muhammad *et al.*[150] found that the amino acid-based IL 1-ethyl-3-methylimidazolium glycinate is also capable of dissolving lignocellulose. Li *et al.*[151] reported that complete dissolution of lignocellulose can be accelerated above the glass transition temperature of lignin (150 °C). By surveying the literature, it can be found that [BMIM][Cl], [AMIM][Cl], [EMIM][Cl] and [EMIM][OAc] are the most used and efficient ILs for dissolving lignocellulosic biomass. Complete biomass dissolution in ILs is dependent on factors optimized for the specific IL–biomass dissolution process. A typical process for the dissolution and regeneration of woody components in an IL is shown in Fig. 23. Generally, the wood is firstly milled and dried, and then added to IL with a certain solid/liquid ratio, and treated at a specified temperature and time while applying mechanical stirring to the mixture. The next step is the regeneration of each fraction with the addition of a precipitating solvent such as water, acetone, dichloromethane, acetonitrile or a mixture. Besides the above mentioned points, the dissolution of lignocellulose in ILs also depends on other factors such as particle size, type of wood, IL to biomass ratio, water content, drying of the IL and pretreatment time.[136,142,149]

3.2 Conversion of biomass to biofuels and chemicals

Due to a high oxygen content of biomass, generally 40–45 wt%,[88] a part of the oxygen should be removed in the form of CO_2 or H_2O so that the lignocellulosic biomass can be converted into high heating value liquid biofuels. Various biofuels and chemicals produced from cellulose, hemicellulose and lignin are shown in Fig. 24.[110] Some of the approaches that employ ILs for the conversion are summarized in the following section.

3.2.1 Conversion of cellulose

Conversion of cellulose to ethanol. Sugars exist in biomass in polymer forms such as cellulose, starch, or hemicellulose and account for approximately 75 wt% of the total biomass. Presently, the production of ethanol by fermentation of sugars is the primary technology for the generation of liquid fuel from biomass. Sugars can be converted to ethanol by fermentation usually with enzymes as shown in the following equation:

$$C_6H_{12}O_6 \rightarrow 2C_2H_5OH + 2CO_2 \quad (5)$$

For conversion to ethanol, the cellulose has to be converted into fermentable sugars first. Although cellulosic biomass mainly consists of sugar units, it needs extensive pretreatment before fermentation, which is one of the main economic costs of producing biofuel. Several approaches have been developed to pretreat cellulosic biomass, including dilute acid treatment, steam explosion, hydrothermal processes, dissolving in organic solvents, enzymatic processes, ammonia fiber explosion, strong alkali processes and highly-concentrated acid treatment.

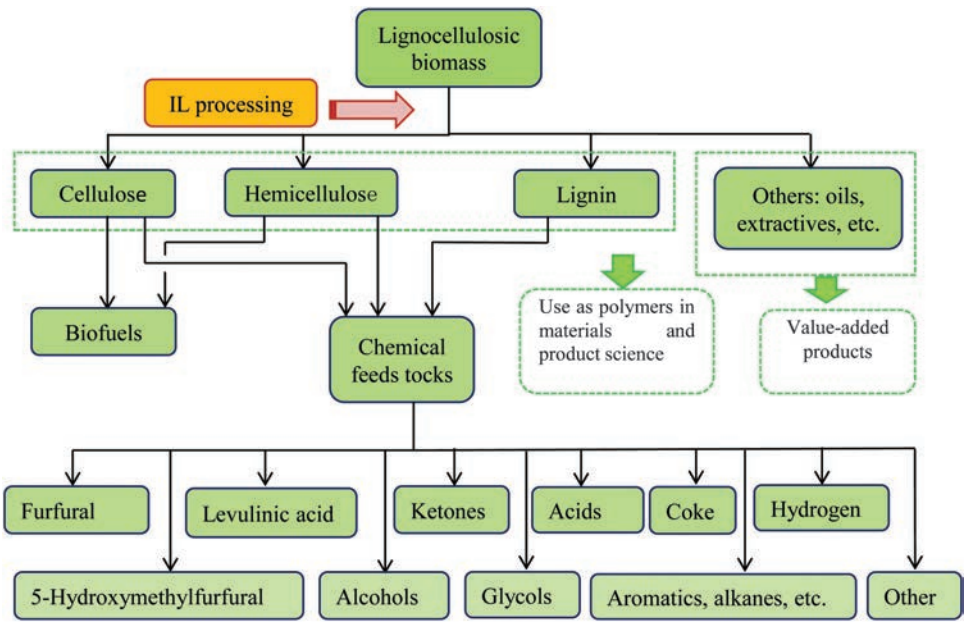

Fig. 24 Possible applications of the three major components from lignocellulosic biomass. Reprinted with permission from ref. 110.

However, there are drawbacks of these methods, including a huge amount of water consumption, high pollution, and high energy consumption.

In recent years, IL pretreatment has become more attractive due to the non-derivatizing nature of ILs, because no fermentation inhibitors are produced and because the products are easily recovered. Several ILs have been proven to be effective in enhancing saccharification. Li *et al.*[152] reported that the total reducing sugar yields are up to 66%, 74%, 81% and 68% for the hydrolysis of corn stalk, rice straw, pine wood and bagasse, respectively when using [BMIM]Cl as the solvent and HCl as the catalyst. The authors also found that the acidic ILs 1-(4-sulfobutyl)-3-methylimidazolium bisulfate [SBMIM][HSO_4] and 1-butyl-3-methylimidazolium bisulfate [BMIM][HSO_4] have dual functions as solvents and catalysts. They hydrolyzed corn stalk in [BMIM]Cl with the addition of the acidic ILs [BMIM][HSO_4] and [SBMIM][HSO_4], resulting in reducing sugar yields of 68% and 71%, respectively.[152] Li *et al.*[153] dissolved wheat straw in [EMIM][OAc], [BMIM]Cl, and several phosphoric ILs including 1-ethyl-3-methyl imidazolium diethyl phosphate ([EMIM][DEP]), 1-ethyl-3-methyl butylpyridinium diethylphosphate ([EMBy][DEP]), and 1-ethyl-3-methyl imidazolium dibutyl phosphate ([EMIM][DBP]), and it was found that [EMIM][DEP] gave the highest yield of reducing sugars of 50% after 1 h pretreatment at 100 °C.

However, it was found that high concentrations of ILs lead to enzyme inactivation in the following fermentation process.[131,154,155] To preserve enzyme activity, a sufficient amount of water is needed. For example, cellulases from *Penicillium janthinellum* remained sufficiently stable for 1 h in up to 50% [BMIM]Cl–H_2O and [BMP]Cl–H_2O solutions.[156,157] In an *in situ* investigation of the enzyme saccharification of cellulose in enzyme compatible [EMIM][DEP] by Kamiya *et al.*,[158] it was reported that when the volume of IL to water was greater than 3 : 2, little cellulase activity was observed, while decreasing the volume ratio to 1 : 4 enabled 70% of the cellulase activity to be maintained.

The conversion of cellulose to ethanol *via* fermentation of sugars is an important approach for the conversion of biomass to biofuel. The microbial conversion of sugars (mono and disaccharides) to ethanol has become well established in the past century.[159–162] However, there are challenges for the pretreatment of cellulose to produce reducing sugars,[163–165] which can be summarized as follows: (1) the development of ILs with low lignin degradation products that hinder the fermentation process; (2) producing highly digestible cellulose for hydrolysis to reducing sugars; (3) the recovery of ILs with low energy consumption and low cost.

Conversion of cellulose to 5-hydroxymethylfurfural (5-HMF). Recently, much attention has been paid to 5-HMF, which is regarded as one of the top building block chemicals obtained from biomass that can be further converted to fuels. For example, hydrogenation of 5-HMF produces 2,5-dimethylfuran, and condensation of 5-HMF followed by hydrodeoxygenation leads to C7–C15 liquid alkanes (eqn (6)).[166]

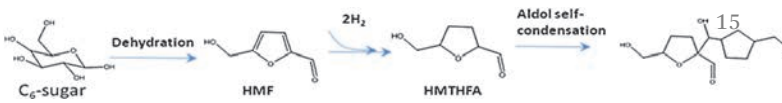

(6)

Despite the versatile applications of 5-HMF, it has not been produced on an industrial scale because of the high production costs. Recently, researchers devoted their efforts to finding an economic route for 5-HMF production. Zhang *et al.*[167] firstly found that the metal halides in [EMIM][Cl] are effective catalysts for the conversion of carbohydrates into 5-HMF. They studied the use of many metal halides and different ILs ([BMIM][Cl], [EMIM][Cl], [OMIM][Cl]) for the dehydration of sugars. The highest yields for the conversions of fructose and glucose to 5-HMF were 83% and 70%, respectively. Zhao *et al.*[168] obtained a high yield for the conversion of glucose into 5-HMF (91%) using a chromium salt and [BMIM][Cl] under microwave irradiation.

In the case of imidazolium based ILs, the alkyl chain and hydrogen bonds are two important factors[169] for 5-HMF production. The cations of ILs with an alkyl chain shorter than four carbons are suitable for 5-HMF preparation because of the low steric hindrance effect, while strong hydrogen bonds formed between the anions and the fructose molecules also lead to high reaction activity.

It is regarded that the isomerization of glucopyranose to fructofuranose is crucial.[167] Zhang *et al.*[167] proposed that the $CrCl_3$ anion plays a role in proton transfer, facilitating mutarotation of glucose in [EMIM]Cl, as shown in Fig. 25. A critical

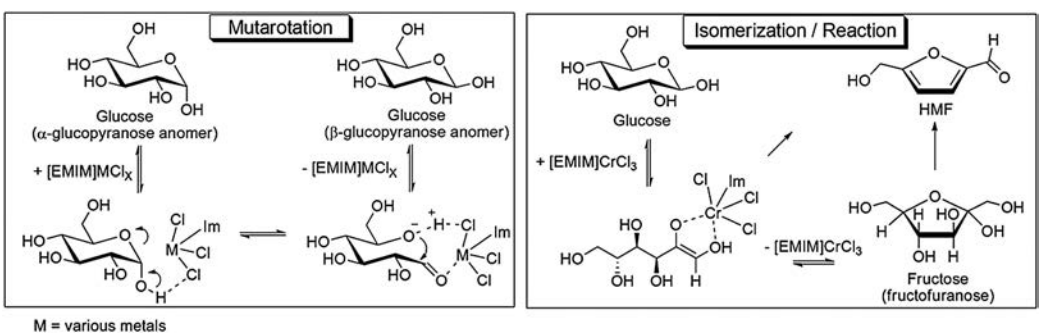

Fig. 25 Mechanism of glucose conversion into 5-HMF by metal halide interaction with [EMIM]Cl. Reprinted with permission from ref. 167.

role of the $CrCl_3$ anion is to affect the formal hydride transfer, leading to the isomerization of glucose to fructose. Once fructose is formed, dehydration of fructofuranose is rapid in the presence of the catalyst in the IL. Other metal halides also bind to glucose, but they promote alternative reaction paths leading to undesired products.

Besides, it has been found that cellulose or even lignocellulosic biomass can be hydrolyzed into 5-HMF directly. Tan *et al.*[170] reported a single-step process for cellulose conversion into 5-HMF with a yield of 55% by using ILs with $CuCl_2$–$CrCl_2$ as catalyst at 120 °C. Qi *et al.*[171] reported a two-step conversion of cellulose into 5-HMF in ILs using acidic resin and $CrCl_3$. In the first step, glucose was produced in high yield from the hydrolysis of cellulose catalyzed by a strong acidic cation exchange resin in ILs with the gradual addition of water. In the second step, the resin was separated from the reaction mixture and $CrCl_3$ was added, which lead to a 5-HMF yield of 73%. Recently, a 5-HMF yield of 51% was obtained from cellulose in an IL–$ZrCl_4$ system in several minutes under microwave irradiation without using $CrCl_3$.[172]

Other valuable chemicals such as glucose esters, sorbitol, and 2,5-dimethylfuran have also been synthesized from cellulose in ILs, and can be used as fuels directly or as precursors.[173,174] Dirk *et al.* reported that α-D-glucose pentaacetate can be produced with a yield of 70% by a two step process.[175] After depolymerization of cellulose, α-D-glucose pentaacetate can be converted into sorbitol as the dominant product in 51–74% yield.

3.2.2 Conversion of hemicellulose. Hemicellulose, a readily available form of biomass, can also be catalytically converted to furans, sugar alcohols, and alkanes for fuels. Hemicellulose can be hydrolyzed in ILs as the solvent and Brønsted/Lewis acid catalysts to xylose. Zhang and Zhao[176] reported the conversion of xylan and lignocellulosic biomass to furans in [BMIM]Cl in the presence of $CrCl_3 \cdot 6H_2O$ under microwave irradiation, in which the yield of furfural from xylan was 63%. Enslow *et al.*[177] reported that hemicellulose can be hydrolyzed to xylose in 90% yield, with 5 wt% dehydration products and 4 wt% humins with water added stepwise. Other chlorides including $FeCl_3$, KCl, $CaCl_2$ and $MgCl_2$ are also effective for the conversion of hemicellulose. Zhang *et al.*[178] found that hydrolysis of xylan into furfural gave a yield of up to 85% when the reaction was carried out at 170 °C for a reaction time of 10 s with $AlCl_3$ as catalyst in [BMIM]Cl. For untreated corncob, grass and pine wood, the reactions catalyzed by $AlCl_3$ produced furfural in yields of up to 19%, 31% and 34%, respectively. By a kinetics study, xylan hydrolysis was found to exhibit faster initial reaction rates than cellulose under similar conditions in ILs[177] because hemicellulose has less structural strength.[179]

3.2.3 Conversion of lignin. Lignin accounts for 18–40% of dry wood. However, lignin has received less attention relative to cellulose and hemicellulose, mainly because of its complex structure and resistance to degradation. As shown in Fig. 26,[180] native lignin consists of aryl ether units connected by an array of ether and alkyl linkages. Cleavage of these linkages would yield monomeric phenols and methoxyphenols.

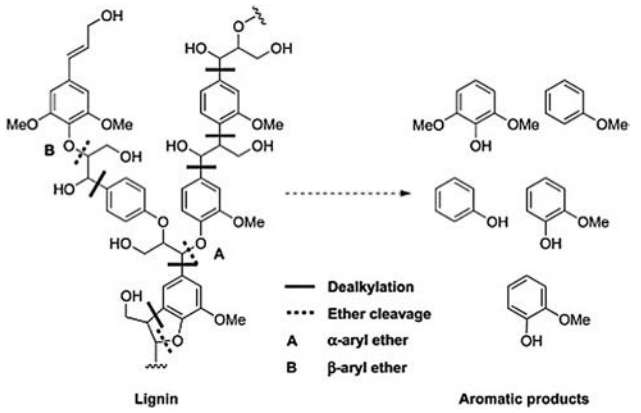

Fig. 26 Generalized chemical structure of lignin and schematic for its conversion into monomeric aromatic products. Reprinted with permission from ref. 180.

The β-O-4 bond is the most dominant cross-link, comprising 45–60% of all monomer linkages present in lignin. Thus, most studies have focused on disruption of the β-O-4 bond by model compounds. For example, the cleavage of two β-O-4-containing model compounds, the phenol-based guaiacylglycerol-*b*-guaiacyl ether and anisole-based veratrylglycerol-β-guaiacyl ether, was reported by Jia *et al.*[181] using metal chlorides in [BMIM]Cl. $FeCl_3$, $CuCl_2$, and $AlCl_3$ were found to be effective for cleaving the β-O-4 linkage, achieving complete cleavage of guaiacylglycerol-*b*-guaiacyl ether after 120 min at 150 °C. The anisole-based veratrylglycerol-β-guaiacyl ether, which lacks the acidic phenolic hydroxide group, has lower reactivity. Using $AlCl_3$, only 75% cleavage of the β-O-4 linkage was achieved under the same conditions.[181] Later, the same research group pointed out that the HCl formed *in situ* by the hydrolysis of metal chlorides catalyzes the β-O-4 bond cleavage.[182] An increase in available water can lead to more β-O-4 bond cleavage of guaiacylglycerol-*b*-guaiacyl ether. About 70–80% of the guaiacylglycerol-*b*-guaiacyl ether β-O-4 bond reacted with water to produce guaiacol at 150 °C after 120 min in the presence of $FeCl_3$, $CuCl_2$, and $AlCl_3$. The acidity of the IL is also correlated with the conversion.[183] The yield of guaiacol in the various ILs followed the order of [HMIM]Cl > [BMIM][HSO_4] > [HMIM]Br > [HMIM][HSO_4] > [HMIM][BF_4].[181]

Most catalytic treatments of lignin or model compounds in ILs require high temperatures, which need extra energy. Electrochemical techniques are an alternative route to drive the reaction at low temperatures. Chen and co-workers[184] first investigated the electrolysis of lignin model compounds at an electrode surface in [BMIM][TFSI]. By using abrasive stripping voltammetry, multiple peaks were observed at different potentials for different lignin model compounds due to the formation of decomposed products. Later, Reichert *et al.* reported the electro-oxidative depolymerization of lignin in [Et_3NH][CF_3SO_2] with ruthenium–vanadium–titanium mixed oxide anode as the catalyst. In this process, a variety of

products, including vanillin, syringic acid, vanillic acid, guaiacol and other identified aromatics were obtained.[185]

There are several highly successful methods for the conversion of lignin model compounds in ILs with near complete conversion and high selectivity by changing the structures of the ILs. However, this is still far away from the research of the applications of these processes using authentic lignin samples. Fundamental models for lignin dissolution and interactions with ILs are still at an early stage of development. The developed processes also produce complex mixtures of products, which are also economically unattractive owing to the cost associated with separation of the mixture from ILs. Future research should be focused on clarify the mechanism of lignin depolymerization at the molecular level and further producing high yields of monomeric aromatics from a wide variety of lignin sources for energy utilization.

4. Photoelectric chemical processes

As one of the important clean energy alternatives, solar energy is reliable and can be theoretically implemented on a large scale.[25] Solar cells are an important way to utilize solar energy. Meanwhile, it is also necessary to develop energy storage devices to realize the effective and practical application of solar cells. As the key factor that affects the performance of photoelectric and energy storage devices, the development of electrolytes with high efficiency and safety is a great challenge that needs urgently to be solved. As unique media with the preeminent properties, ILs are an indispensable component to achieve green photoelectric chemical processes.

4.1 Solar energy (dye-sensitized solar cells)

Dye-sensitized solar cells (DSCs) have attracted significant attention due to their high efficiency, low cost, and simple fabrication processes.[186] Typically, a DSC is composed of a photoanode with various nanosemiconductors (TiO_2 is the most common) and the corresponding dyes, electrolyte and a counter electrode (Fig. 27). The working principle can be simply described as follows: first, the photo-excitation of the dye induces the injection of electrons into the conduction band of TiO_2 and the electrons are then collected by the substrate and transferred to the counter electrode through the external load. The regeneration of dyes is realized by reduction reactions with the redox couple (iodide) in the electrolyte. The iodide can be regenerated in turn by the reduction of triiodide at the counter electrode, thus completing the circuit. A recorded efficiency of over 12% has been achieved based on a liquid electrolyte.[187,188] However, the disadvantages of traditional organic electrolytes, such as leakage and volatilization, difficulty in sealing and instability, are considered as the critical factors limiting the long-term performance and outdoor use of DSCs. As an alternative media with excellent physicochemical properties, IL-based electrolytes have been widely investigated.[189,190] This section will summarize the recent progress on the development of IL-based electrolytes, quasi-solid-state and solid-state electrolytes of DSCs.

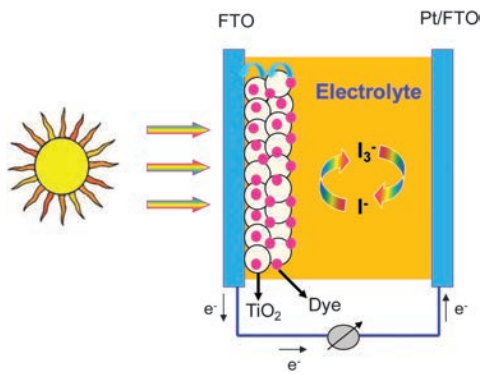

Fig. 27 The structure diagram of a DSC.

4.1.1 Ionic liquid electrolytes

Imidazolium ILs. Papageorgiou *et al.* first introduced [HMIM]I (list of acronyms can be found in Table 2) into the electrolyte system of a DSC.[191] The device showed superior stability but low conversion efficiency. To further improve the efficiency of the device, various kinds of ILs were developed. The representative ILs are imidazolium, pyridinium, alkylpyrrolidinium, quaternary alkylammonium, and alkylphosphonium type cations with halide (Cl^-, Br^-, I^-), polyatomic inorganic ($[PF_6]^-$, $[BF_4]^-$), organic anions ($[NO_3]^-$, $[TFSI]^-$, $[Tf]^-$) and so on. However, the conversion efficiency of the device is restricted due to the high viscosity, low conductivity and poor fluidity caused by unitary IL electrolytes.

To solve these problems, a series of binary and ternary IL electrolytes have been developed.[192–196] A binary IL electrolyte system based on [PMIM]I/[EMIM][DCN] combined with Z907 dye was investigated by Grätzel's group (Fig. 28). A conversion efficiency of 6.6% was obtained at an irradiance of one sun (100 mW cm^{-2}).[192] Subsequently, they suggested another binary IL ([PMIM]I/[EMIM][NCS] electrolyte system to solve the instability of [EMIM][DCN] and the resulting efficiency was 7.0%.[193] Then [PMIM]I/[EMIM][TCM] mixed electrolyte combined with N907Na dye exhibited an efficiency of 7.4%.[194] Then, ternary eutectic melt electrolytes were developed by Wang and coworkers. An efficiency of 7.1% under one sun irradiation was achieved with the ternary IL electrolyte [DMIM]I/[EMIM]I/[AMIM]I, with I_2, additives of guanidinium thiocyanate (GNCS) and *N*-butylbenzoimidazole (NBB) using N907Na sensitizer (Fig. 29, device A). The corresponding open circuit voltage (V_{oc}), short circuit photocurrent density (J_{sc}) and fill factor (FF) are 721 mV, 12.82 mA cm^{-2} and 0.768, respectively. A higher efficiency of 8.2% was achieved with another ternary eutectic melt electrolyte [DMIM]I/[EMIM]I/[EMIM][TCB]/I_2/GNCS/NBB (Fig. 29, device B).[195] The corresponding photovoltaic parameters (V_{oc}, J_{sc}, FF) for device B are 741 mV, 14.26 mA cm^{-2} and 0.774, which are higher than those of device A. The mechanism investigation showed that the more positive Nernst potential, slower charge recombination rates, larger effective electron diffusion coefficients (D) and higher charge collection yield contributed to the superior photovoltaic performance of device B compared with device A. Furthermore, superior long

Table 2 List of acronyms for the ILs and polymers

Acronyms	ILs/polymers
[HMIM]I	1-Methyl-3-hexylimidazolium iodide
[PMIM]I	1-Methyl-3-propylimidazolium iodide
[EMIM][DCN]	1-Methyl-3-ethylimidazolium dicyanamide
[EMIM][NCS]	1-Ethyl-3-methylimidazolium thiocyanate
[EMIM][TCM]	1-Ethyl-3-methylimidazolium tricyanomethanide
[DMIM]I	1,3-Dimethylimidazolium iodide
[EMIM]I	1-Ethyl-3-methylimidazolium iodide
[AMIM]I	1-Allyl-3-methylimidazolium iodide
[EMIM][TCB]	1-Ethyl-3-methylimidazolium tetracyanoborate
[EMIM][$B(CN)_4$]	1-Ethyl-3-methylimidazolium tetracyanoborate
[BMIMB]Br	3-(4-(Benzimidazolyl)butyl)-1-methylimidazolium bromide
[BMIMB][BF_4]	3-(4-(Benzimidazolyl)butyl)-1-methylimidazolium tetrafluoroborate
[EMIM][SCN]	1-Ethyl-3-methylimidazolium thiocyanate
[EMIM][McMT]	(1-Ethyl-3-methylimidazole-modified mercapto-5-methyl-1,3,4-thiadiazole)
[DMPIM]I	1,2-Dimethyl-3-propylimidazolium iodide
[TMIM]Cl	1-Methyl-3-[(triethoxysilyl)propyl]imidazolium chloride
$P_{12}I$	1-Ethyl-1-methyl pyrrolidinium iodide
[EMIM][FSI]	1-Ethyl-3-methylimidazolium bis(fluorosulfonyl)imide
[ETMIM][TFSI]	1-Ethyl-2,3-trimethylene imidazolium bis(trifluoromethane sulfonyl)imide
[$MEMBu_3P$][TFSI]	1-Methoxyethoxymethyl(tri-*n*-butyl) phosphonium bis(trifluoromethane sulfonyl)imide
[PP13][TFSI]	1-Methyl-1-propylpiperidinium bis(trifluoromethane sulfonyl)imide
[PYR_{14}][FSI]	*N*-Butyl-*N*-methylpyrrolidinium bis(fluorosulfonyl)imide
[$Py_{1,4}$][TFSI]	*N*,*N*-Methyl butyl pyrrolidinium bis(trifluoromethanesulphonyl) imide
[PYR_{13}][FSI]	*N*-Propyl-*N*-methylpyrrolidinium bis(fluorosulfonyl) imide
[TEA][BF_4]	Tetraethylammonium tetrafluoroborate
[Bu_3HP][BF_4]	Tributylphosphonium tetrafluoroborate
[Me_3S][TFSI]	Trimethylsulfonium bis(trifluorosulfon)imide
P([MOEMIM]Cl)	Poly(1-oligo (ethylene glycol) methacrylate-3-methyl imidazolium chloride)
PEGDME	Polyethylene glycol dimethyl ether
P-HI	P[((3-(4-vinylpyridine) propanesulfonic acid) iodide)-*co*-(acrylonitrile)]
[PBVIM][TFSI]	Poly(1-butyl-3-vinylimidazolium bis(trifluoromethanesulfonyl)imide)
PVPPEGMEI	Poly(*N*-poly(ethylene glycol)-4-vinylpyridinium iodide)
PEBII	Poly((1-(4-ethenylphenyl)methyl)-3-butyl-imidazolium iodide)
PVC-*g*-POEM	Poly(vinyl chloride)-*g*-poly(oxyethylene methacrylate)
PAAII	Poly(1-alkyl-3-(acryloyloxy) hexylimidazolium iodide)
PEAII	Poly(1-ethyl-3-(acryloyloxy)hexylimidazolium iodide)
PSPEO-PS	Poly(styrene-*block*-ethylene oxide-*block*-styrene)
PVdF-HFP	Poly(vinylidene fluoride-*co*-hexafluoropropylene)

term stability of device B was obtained under successive irradiance of AM 1.5G at 60 °C. The retained efficiency was 93% of its initial value over 1000 h (Fig. 30).

The heteroleptic polypyridyl ruthenium sensitizer C103 (Fig. 28) with high molar extinction coefficient was developed for DSCs based on low-volatility electrolyte (0.15 M I_2, 1.0 M [DMIM]I, 0.5 M NBB, 0.1 M GNCS in 3-methoxypropionitrile (MPN)) and IL electrolyte ([DMIM]I/[EMIM]I/[EMIM][TCB]/I_2/NBB/GNCS, 12/12/16/1.67/3.33/0.67, molar ratio).[196] The photovoltaic parameters (V_{oc}, J_{sc}, FF, efficiency (η)) of the MPN-based device were 771 mV, 17.51 mA cm^{-2}, 0.709 and 9.6%, respectively. The IL-based device showed an efficiency of 8.5%, which is comparable to that of the MPN-based device. Higher efficiencies of 9.1 and 8.9% were achieved under the lower light intensity of 9.4 mW cm^{-2} and 51.3 mW cm^{-2}, respectively (Fig. 31). The superior long term stability was confirmed with the efficiency remaining at 94% of its initial value over a period of 1000 h under the successive irradiance of full sunlight at 60 °C.

Besides the ruthenium sensitizers, metal-free organic dyes have also been investigated in IL electrolyte systems due to their high molar extinction coefficients. Kuang *et al.* reported the molecularly tailored indoline sensitizers D102, D149 and D205 (Fig. 28) for the binary IL electrolyte of [PMIM]I/[EMIM][$B(CN)_4$].[197] Efficiencies of 4.86, 6.38 and 7.18% were obtained for D102, D149 and D205, respectively. The high photovoltaic performance of D205 was assigned to the structure with the octyl chain, which suppressed electron recombination and enhanced electron lifetime (τ). Polyene-diphenylaniline-based organic dyes (D5, D7, D9 and D11, Fig. 28) combined with the same binary IL electrolyte gave conversion efficiencies from 4.6 to 6.5%. The D11-based device exhibited the highest efficiency due to it having the longest electron lifetime, which is regarded as one of the key efficiency-determining factors to determine the recombination dynamics of solar cells.[198] Wang's group developed the organic dyes C204 with 3,4-ethylenedioxythiophene (EDOT) and C205 with biEDOT units (Fig. 28), which showed remarkably red-shifted photocurrent spectral responses compared to their thiophene and bithiophene counterparts.[199] The corresponding devices exhibited efficiencies of 7.31% for C204 and 7.61% for C205 based on ternary IL electrolyte ([DMIM]I/[EMIM]I/[EMIM][TCB]/I_2/NBB/GNCS (molar ratio: 12/12/16/1.67/3.33/0.67)). Excellent long term stabilities were also achieved with the efficiencies being

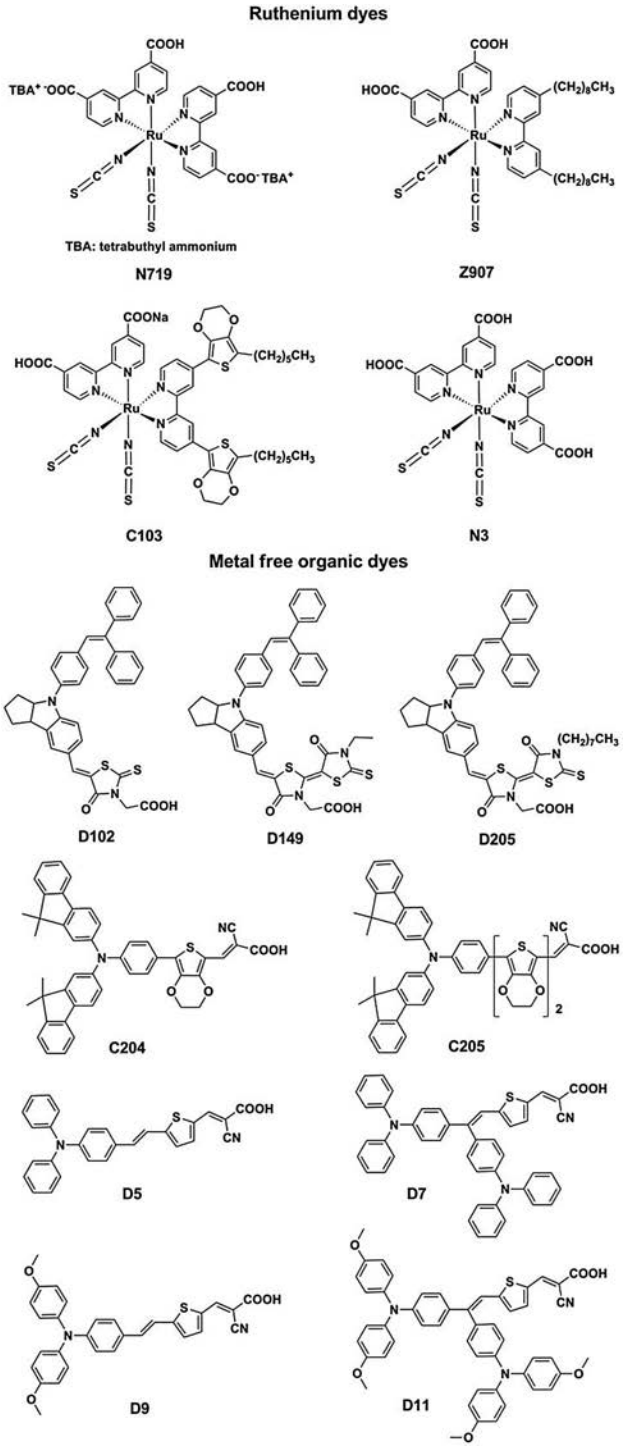

Fig. 28 The structures of sensitizers used with IL-based electrolytes.

maintained at over 92% of their initial values after 1000 h of successive full sunlight at 60 °C.

Other types of ILs. Apart from the frequently used imidazolium-based ILs, other types of ILs have also been investigated for the electrolyte systems of DSCs, as shown in Fig. 32. A series of quaternary ammonium iodides, $[Me_2Pe_2N]I$,

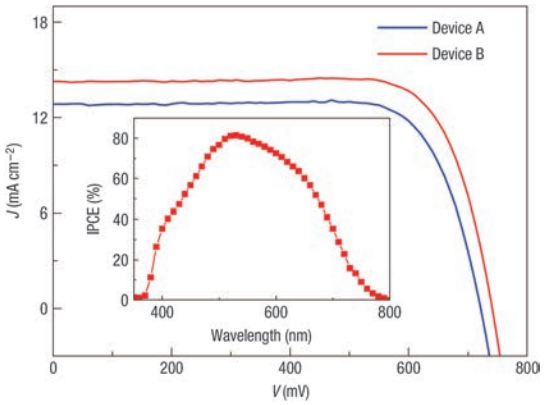

Fig. 29 The *I*–*V* curves of device A (electrolyte composition: [DMIM]I : [EMIM]I : [AMIM]I : I_2 : NBB : GNCS = 8 : 8 : 8 : 1 : 2 : 0.4, molar ratio) and device B (electrolyte composition: [DMIM]I : [EMIM]I : [EMIM][TCB] : I_2 : NBB : GNCS = 12 : 12 : 16 : 1.67 : 3.33 : 0.67, molar ratio) with the incident photon-to-current conversion efficiency (IPCE) spectrum of device B as the insert figure. Reprinted with permission from ref. 195.

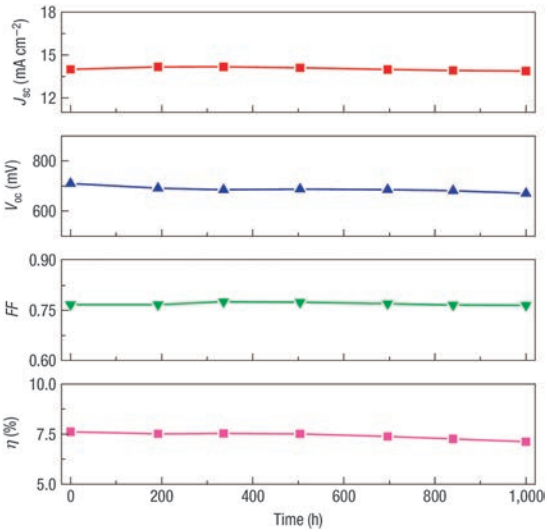

Fig. 30 The long term photovoltaic performance of device B under successive irradiance of AM 1.5G at 60 °C. Reprinted with permission from ref. 195.

$[Me_2Hex_2N]I$, $[Et_2Pe_2N]I$ and $[Et_2Hex_2N]I$, were synthesized by Santa-Nokki *et al.*[200] Efficiencies of 2.4 and 2.3% were obtained with the flow state electrolyte (0.5 M TBP, $[Me_2Hex_2N]I : I_2$ = 10 : 1, weight ratio) and the soft solid state electrolyte (0.5 M TBP, $[Et_2Hex_2N]I : I_2$ = 10 : 1, weight ratio) under illumination of 10 mW cm^{-2}. Cai *et al.* investigated IL electrolytes based on *N*-methyl-*N*-allylpyrrolidinium cations ($[P13']^+$) combined with I^-, $[NO_3]^-$, $[NCS]^-$, and $[DCA]^-$.[201] Compared with the $[P13'][NO_3]$ and [P13′][NCS]-based electrolytes, the highest efficiency of 5.58% was achieved with a V_{oc} of 719 mV, J_{sc} of 10.94 mA cm^{-2}, and FF of 0.709 for the [P13′][DCA]-based electrolyte ([P13′]I/[P13′][DCA]/I_2/NBB/GNCS). The intensity modulated photovoltage spectroscopy (IMVS)/intensity modulated

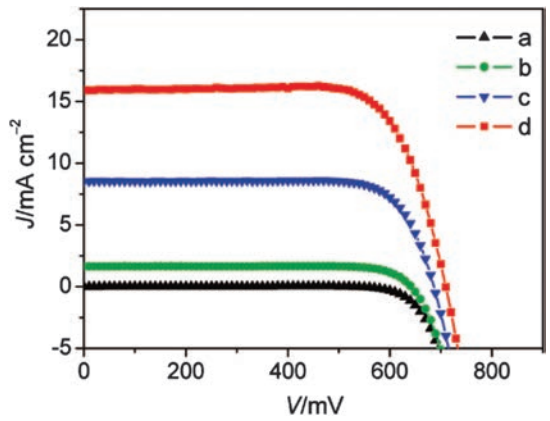

Fig. 31 The *I–V* curves of the device based on IL electrolyte (DMIMI : EMIMI : [EMIM][TCB] : I_2 : NBB : GNCS = 12 : 12 : 16 : 1.67 : 3.33 : 0.67 (molar ratio)) under different light intensities: (a) in dark; (b) 9.4 mW cm^{-2}; (c) 51.3 mW cm^{-2}; (d) 99.8 mW cm^{-2}. Reprinted with permission from ref. 196.

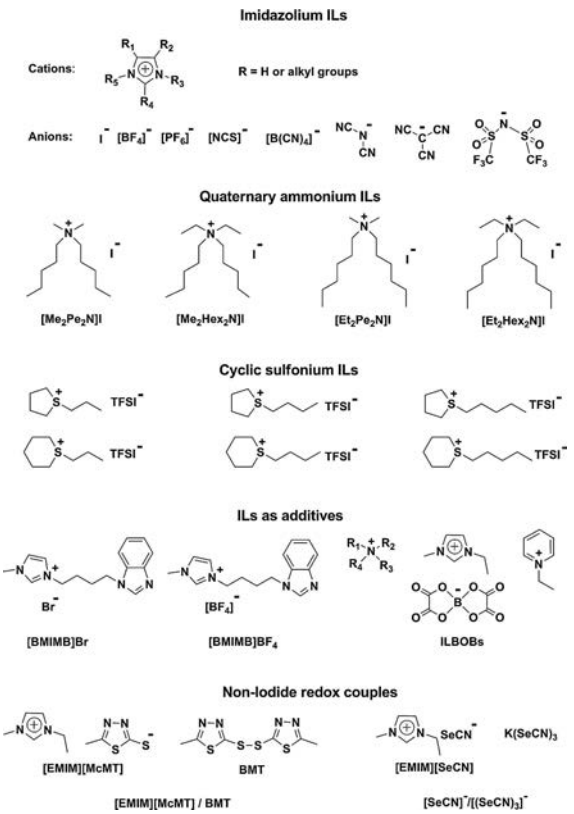

Fig. 32 The structures of ILs used in the electrolyte systems of DSCs.

photocurrent spectroscopy (IMPS) measurements showed that the higher electron lifetime and electron diffusion coefficient, as well as the electron diffusion length (L) resulted in more efficient charge collection and electron transport, and thus the superior photovoltaic performance was acquired. Dai's group have developed a series of sulfonium-based ILs for electrolytes.[202,203] The structures of hydrophobic ILs of cyclic sulfonium cations with [TFSI]$^-$ are shown in Fig. 32.[202] The devices based on the five-ring ILs with different alkyl chain lengths showed slightly higher conversion efficiencies and faster triiodide ion diffusion than the six-ring ones. Chronoamperometry measurements showed that the shorter substitute benefited ion diffusion. *S*-Propyltetrahydrothiophenium iodide ([T_3]I) was applied in a DSC as the solvent and the iodide ion source of the electrolyte (0.35 M I_2, 0.1 M LiI, 0.5 M *N*-methylbenzimidazole (NMBI) in [T_3]I).[203] A conversion efficiency of 3.51% was achieved, which is better than most of the trialkylsulfonium iodides in DSCs, showing the importance of designing the structures of ILs.

Beside the above ILs, another type of IL–metal complex (ILMC, 1-(1-carboxyethyl)-3-methylimidazolium bromide coupled with an Eu center) electrolyte system was developed by Zhang's group. The ILMC-based device exhibited superior photovoltaic performance compared with the typical imidazole IL ([PMIM]I).[204] A conversion efficiency of nearly 7% was achieved without any additives, which represents a significant improvement of 69.2% compared with the value of 4.13% for the IL electrolyte without a metal centre (Fig. 33a). The mechanism investigations demonstrated that the higher conductivity (Fig. 33b), suppressed recombination reactions and the longer electron lifetime of the ILMC electrolyte contribute to the superior photovoltaic performance.

Additives in IL electrolytes. Benzimidazolyl functionalized ILs of [BMIMB]Br and [BMIMB][BF_4] were synthesized and applied as additives in the IL electrolyte systems for DSCs.[205] Conversion efficiencies of 6.50 and 6.31% were obtained for [BMIMB]Br- and [BMIMB][BF_4]-based devices under one sun illumination, respectively, which were higher than the values with traditional additives (6.20% for NBB and 6.29% for TBP). The improved efficiency was ascribed to the suppression of charge recombination. While decreasing the sunlight irradiation intensity to 0.5 sun, the [BMIMB]Br- and [BMIMB][BF_4]-based devices exhibited increasing efficiencies of 7.79 and 7.67%, respectively. Another series of bis(oxalate)borate-based ILs (ILBOBs, Fig. 32) were introduced into the electrolyte system of a DSC as additives by Wang *et al.*[206] The photovoltaic performance of the corresponding devices were improved from 26% to 45% in acetonitrile electrolytes compared with the non-additive one, in which the highest efficiency of 8.73% was obtained for [EMIM][BOB]. Subsequently, the IL electrolyte system based on [PMIM]I/[EMIM][BOB] (3 : 1, volume ratio) exhibited a higher efficiency of 5.38% than the value with pure [PMIM]I electrolyte (3.48%), which showed the superior performance of [EMIM][BOB]. The results shown in Fig. 34 gave direct proof of the excellent long term stability of the ILBOB-based electrolyte compared with traditional organic solvents.

Redox couples in IL electrolytes. The redox couple [SeCN]$^-$/[$(SeCN)_3$]$^-$ was employed as an alternative to the traditional I^-/I_3^- couple. The corresponding IL electrolyte was composed of 0.15 M K$(SeCN)_3$, 0.1 M GNCS, and 0.5 M NMBI in [EMIM][SeCN].[207] A determined viscosity of 25 cP (21 °C) and conductivity of 14.1 mS cm^{-1} were obtained for [EMIM][SeCN], which

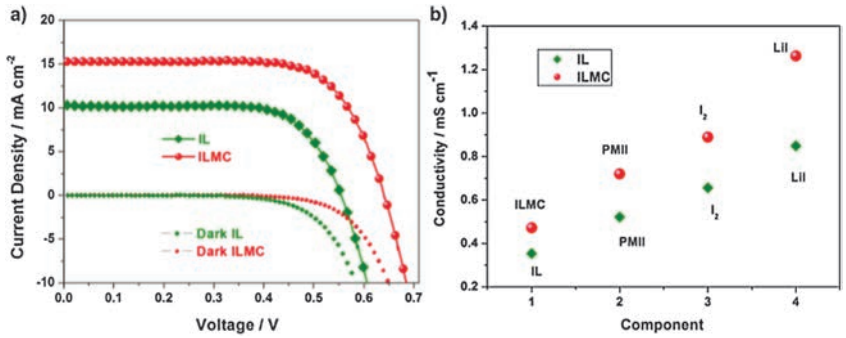

Fig. 33 (a) The *I*–*V* curves and corresponding dark current curves of IL and ILMC-based DSCs. (b) The conductivity of the conductors based on IL and ILMC. Component 1 represents IL or ILMC, and 2, 3 and 4 were prepared by adding [PMIM]I, 0.1 M I_2, and 0.1 M LiI into the former, respectively. Reprinted with permission from ref. 204.

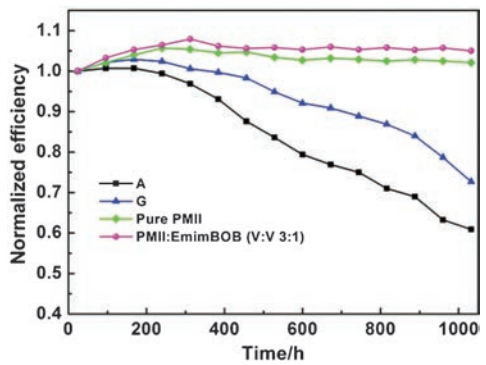

Fig. 34 The stability of DSCs based on electrolyte A (0.05 M I_2, 0.1 M LiI, 0.5 M TBP in acetonitrile), electrolyte G (0.05 M I_2, 0.1 M LiI, 0.5 M TBP, 0.1 M [EMIM][BOB] in acetonitrile), pure [PMIM]I electrolyte (0.1 M I_2 and 0.1 M LiI in [PMIM]I), and hybrid IL electrolyte (0.1 M I_2, 0.1 M LiI in [PMIM]I/[EMIM][BOB] (3 : 1, volume ratio)). Reprinted with permission from ref. 206.

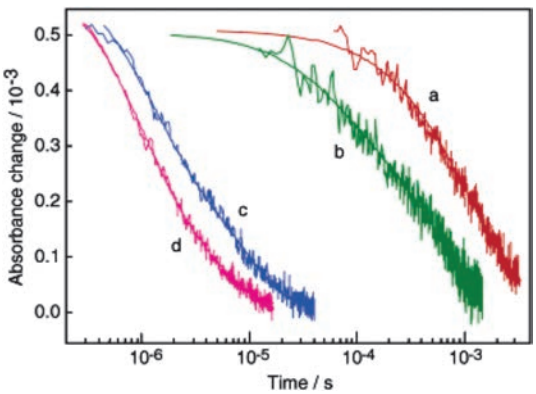

Fig. 35 Transient absorbance decay kinetics of the oxidized state-Z907 dye anchored on TiO_2 film in the presence of pure ILs: (a) [EMIM][DCN]; (b) [EMIM][SCN]; (c) [PMIM]I; (d) [EMIM][SeCN]. Reprinted with permission from ref. 207.

were much better than the most commonly used [PMIM]I (880 cP at room temperature and 0.5 mS cm^{-1}). The diffusion coefficients of $[SeCN]^-$ and $[(SeCN)_3]^-$ are 2.80×10^{-6} and 1.28×10^{-6} cm^2 s^{-1}, respectively, which are about 9 and 7 times higher than the respective values for I^- and I_3^- in [PMIM]I. Fig. 35 shows the temporal behavior of oxidized Z907 dye (650 nm absorption) with [EMIM][SeCN], [PMIM]I, [EMIM][SCN] and [EMIM][DCN], in which [EMIM][SeCN] exhibits the shortest half-life time ($\tau_{1/2}$) of 1.5 μs, indicating the efficient interception of charge recombination of the [SeCN] anion.[207] All the mentioned points above contribute to the high photovoltaic performance of the $[SeCN]^-/[(SeCN)_3]^-$-based IL electrolyte with a high efficiency of 7.5% under AM 1.5 light levels (99.7 mW cm^{-2}).

On the other hand, the organic thiolate/disulfide redox couple [EMIM][McMT]/BMT (Fig. 31) was also developed.[208,209] The corresponding IL electrolyte (0.2 M BMT in [EMIM][McMT]) combined with a poly(3,4-ethylenedioxythiophene) (PEDOT) counter electrode exhibited an efficiency of 3.4% under 0.1 sun.[196] The subsequent device with the IL electrolyte (0.2 M [EMIM][McMT], 0.2 M BMT and 0.5 M NBB in [EMIM][TCB]) and CoS counter electrode showed an efficiency of 4.4% (0.1 sun), which was equivalent to the value of the liquid electrolyte.[197] Table 3 summarizes the detailed information on the IL electrolytes in this section.

4.1.2 Quasi-solid-state electrolytes. To further facilitate the sealing of DSCs, IL-based quasi-solid-state electrolytes can be obtained mainly *via* the following methods: introducing inorganic material or organic polymer and gelator to solidify the IL electrolytes, or *in situ* polymerization or cross-linking of monomers in the ILs. The photochemically and electrochemically stable silica nanoparticles were selected as the gelator of [PMIM]I-based electrolytes by Wang *et al.*[210] Due to the particle size of the silica nanoparticles being smaller than the pores of TiO_2 films, there will be no transmission problem for the quasi-solid-state electrolyte to enter the mesoporous film. The silica-based gel electrolyte (5 wt% SiO_2, 0.5 M I_2, 0.45 M NMBI in pure [PMIM]I) combined with Z907 exhibited a slightly higher conversion efficiency of 6.1% than that of the non-silica one (6.0%) under one sun irradiation. Furthermore, the two electrolytes showed similar diffusion coefficients of I^- and I_3^-. A voltammogram investigation gave further proof that both I^- and I_3^- can move freely in the channels of the silica network. α-TiP was

Table 3 The IL-based electrolytes for DSCs

Authors	Electrolyte	Light intensity (mW cm^{-2})	Dye	V_{oc} (mV)	J_{sc} (mA cm^{-2})	FF	η (%)	Ref.
Wang *et al.*	0.1 M I_2, 0.1 M LiI, 0.45 M NMBI in [PMIM]I/[EMIM][DCN] (13 : 7, volume ratio)	100	Z907	707	12.8	0.727	6.6	192
Wang *et al.*	0.2 M I_2, 0.14 M GuSCN, 0.5 M TBP in [PMIM]I/[EMIM][NCS] (13 : 7, volume ratio)	100	Z907	746	13.3	0.72	7.0	193
Wang *et al.*	0.2 M I_2, 0.5 M NMBI in [PMIM]I/[EMIM][TCM] (1 : 1, volume ratio)	100	Z907Na	752	12.8	0.764	7.4	194
Bai *et al.*	[DMIM]I/[EMIM]I/[EMIM][TCB]/I_2/NBB/GNCS (12 : 12 : 16 : 1.67 : 3.33 : 0.67, molar ratio)	100	Z907Na	741	14.26	0.774	8.2	195
Shi *et al.*	[DMIM]I/[EMIM]I/[EMIM][TCB]/I_2/NBB/GNCS (12 : 12 : 16 : 1.67 : 3.33 : 0.67, molar ratio)	99.8	C103	710	15.93	0.747	8.5	196
Kuang *et al.*	0.2 M I_2, 0.5 M NBB, 0.1 M GNCS in [PMIM]I/[EMIM][B(CN)$_4$] (65 : 35, volume ratio)	100	D205	728	13.73	0.719	7.2	197
Kuang *et al.*	0.2 M I_2, 0.5 M NBB, 0.1 M GNCS in [PMIM]I/[EMIM][B(CN)$_4$] (65 : 35, volume ratio)	100	D11	714	12.40	0.73	6.5	198
Xu *et al.*	[DMIM]I/[EMIM]I/[EMIM][TCB]/I_2/NBB/GNCS (12 : 12 : 16 : 1.67 : 3.33 : 0.67, molar ratio)	100	C205	696	14.85	0.736	7.61	199
Santa-Nokki *et al.*	0.5 M TBP, [Me_2Hex_2N]I/I_2 (10 : 1, weight ratio)	10	N719	600	0.80	0.49	2.4	200
Cai *et al.*	[P13′]I/[P13′][DCA]/I_2/NBB/GNCS (24 : 16 : 1.67 : 3.33 : 0.67, molar ratio)	100	Z907Na	719	10.94	0.709	5.58	201
Guo *et al.*	0.3 M I_2, 0.1 M LiI, 1.5 M [PMIM]I, 0.5 M TBP in [S_{53}][TFSI]	100	N719	640	8.58	0.60	3.27	202
Guo *et al.*	0.35 M I_2, 0.1 M LiI, 0.5 M NMBI in T_3I	100	N719	610	11.22	0.51	3.51	203
Miao *et al.*	0.1 M I_2, 0.1 M LiI, [PMIM]I/ILMC (3 : 1, volume ratio)	100	N719	640	15.28	0.715	6.99	204
Zhao *et al.*	[DMIM]I/[EMIM]I/[EMIM][TCB]/I_2/[BMIMB]Br/GNCS (12 : 12 : 16 : 1.67 : 3.33 : 0.67, molar ratio)	100	Z907	636	15.17	0.674	6.50	205
Wang *et al.*	0.1 M I_2 and 0.1 M LiI in [PMIM]I/[EMIM]BOB (3 : 1, volume ratio)	100	N719	593	13.91	0.65	5.38	206
Wang *et al.*	0.15 M K(SeCN)$_3$, 0.1 M GNCS, 0.5 M NMBI in [EMIM][SeCN]	99.7	Z907	699	14.56	0.735	7.5	207
Tian *et al.*	0.2 M BMT in [EMIM][McMT]	10	TH305	652	0.82	0.65	3.4	208
Tian *et al.*	0.2 M [EMIM][McMT], 0.2 M BMT, 0.5 M NBB in [EMIM][TCB]	10	D35	620	1.04	0.68	4.4	209

also introduced into the binary [PMIM]I/[EMIM][BF_4] system (13 : 7, volume ratio) to construct a composite electrolyte. An improved efficiency of 6.05% was achieved for the α-TiP-based device, which was higher than the value of 3.56% for the non-α-TiP one. The improved efficiency was attributed to the intercalation of [PMIM]$^+$ into α-TiP, leading to an increased diffusion coefficient for I_3^-, suppressed electron recombination and improved electron lifetime.[211] Another composite electrolyte comprising polyaniline-loaded carbon black (PACB) and [PMIM]I achieved a conversion efficiency of 5.81%.[212] When a binary IL system ([EMIM][SCN] : [PMIM]I, 35 : 65, volume ratio) was introduced instead of [PMIM]I, a higher efficiency of 6.15% was obtained with superior stability at 70 °C.[212] An interesting mimetic thixotropy sol–gel electrolyte was investigated by Jin *et al.*, which was composed of 0.05 M I_2, 0.1 M LiI and 0.45 M NMBI in MPN/[PMIM]I (1 : 2, volume ratio) with titania precursor colloid (TPC).[213] It can maintain a reversible transformation between solution and gel, which depends on the disturbance.[213] This thixotropy property facilitated the filling of electrolyte into the TiO_2 film. A high efficiency of 6.45% was achieved based on the obtained thixotropy titania precursor nanocomposite electrolyte (TPNE).

Two kinds of cross-linked gel electrolyte precursors, polypyridyl-pendant poly(amidoamine) dendritic derivative (PPDD) and difunctional halogen derivative (DHD) of poly(ethylene oxide) with iodide on the chain ends ($I(CH_2CH_2O)_nCH_2CH_2I$), were developed as necklace-like polymer electrolytes of DSCs.[214] A conversion efficiency of 6.42% was achieved based on a gelled electrolyte with 10 wt% of precursors (PPDD : DHD = 1 : 2, molar ratio) in a mixed system ([HMIM]I : MPN = 13 : 7, volume ratio), while the corresponding value of the liquid system was 7.0%. The still high performance of the gel electrolyte can be attributed to the special structure of the dendrimers, and the interactions between TiO_2 and ethylene oxide, as well as the polarity effect of the ethylene oxide group. The cross-linking necklace-like structure of the polymer electrolyte has been verified by atomic force microscopy (AFM) with a chain of DHD and beads of PPDD. Another IL polymer, P([MOEMIM]Cl), was also introduced to solidify a binary IL electrolyte (0.5 M I_2, 1 M LiI, 0.5 M NMBI in [HMIM]I/[EMIM][BF_4], weight ratio 2 : 1). The corresponding electrolyte showed a conversion efficiency of 6.1%.[215] Besides these polymers, a low molecular weight gelator (DMBS) derived from the reaction of 3,4-dimethyl-benzaldehyde and D-sorbitol was also developed. The IL gel electrolyte was composed of DMBS in [EMIM][BF_4] with 0.05 M I_2, 0.5 M LiI, 0.4 M [DMPIM]I and 0.5 M TBP.[216] The gelation of the IL was investigated by polarized optical microscopy (POM) (Fig. 36). The results indicated that the IL molecules were immobilized by capillary forces in three-dimensional networks. The gel IL electrolyte exhibited a similar efficiency of 3.63% to the value of 3.83% for the IL electrolyte.

In situ photopolymerization is regarded as an important way to prepare quasi-solid-state electrolytes for DSCs. Meng's group reported the *in situ* photopolymerization of the precursor 1,6-hexanediol diacrylate (HDDA) in [HMIM]I.[217] The oligomer PEGDME was introduced to improve the miscibility between IL and polymer. The PHDDA/[HMIM]I/PEGDME/I_2 electrolyte

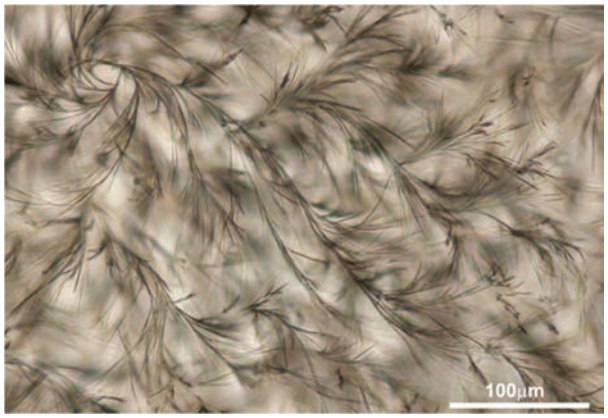

Fig. 36 POM image of the [BMIM][BF_4] gel combined with 1 wt% of DMBS. Reprinted with permission from ref. 216.

exhibited an efficiency of 5.83% under 100 mW cm^{-2} and showed good long term stability. PEGMDE played an important role in increasing the conductivity of the electrolyte, reducing the interfacial contact resistance, improving the interfacial electron transfer and diffusion of the redox species, and enhancing the electron lifetime in the TiO_2 film.

Poly(ILs) are another kind of potential alternative for highly efficient electrolytes. The acidic IL polymer P-HI has been developed in IL electrolyte ([HMIM]I/[AMIM]I/NMBI/GNCS, molar ratio: 8 : 8 : 1.2 : 1.2).[218] The composite electrolyte with 20 wt% P-HI exhibited an efficiency of 6.95% under 100 mW cm^{-2}, which was higher than the value of 6.45% for the non-P-HI electrolyte. The improvement in the electrolyte was attributed to the electrostatic forces of the sulfonic acid group from P-HI, which with the IL form a homogeneous and continuous framework, thus enhancing the transportation of redox couples in the electrolyte. An electrolyte based on [PBVIM][TFSI] combined with 0.1 M I_2, 0.1 M LiI, and 0.5 M TBP in [PMIM]I/[EMIM][TFSI] (13 : 7, volume ratio) yielded a conversion efficiency of 4.4% with superior long-term stability.[219] A [PBVIM][TFSI]-based electrolyte (0.1 M I_2, 0.5 M TBP, 0.1 M GNCS, [EMIM]I/[PMIM]I/[EMIM][SCN] (6 : 6 : 7, volume ratio), with 25 wt% of [PBVIM][TFSI], and 15 wt% of IL–TiO_2 nanoparticles (by tethering [TMIM]Cl to TiO_2 nanoparticles) achieved an overall conversion efficiency of 5.26% under one sun irradiation.[220] Correspondingly, a lower efficiency of 4.89% was obtained for the non-IL–TiO_2-based device. The results showed that the IL–tethered TiO_2 nanoparticles in poly(IL)-based electrolyte was a successful strategy to further improve the J_{sc} and V_{oc} of the device, due to the increased ionic conductivity and diffusion coefficients of I_3^-. The detailed information is summarized in Table 4.

4.1.3 Solid-state electrolytes. To solve the main problem of the poor pore-filling and imperfect contact between photoanodes and solid-state electrolytes, many efforts have been devoted to developing new types of highly-efficient solid-state electrolytes. Alkyloxy-imidazolium iodide ionic polymer (AIIP) was combined with [DMPIM]I, I_2 and SiO_2 to fabricate an all-solid-state electrolyte.[221] Fig. 37 schematically presents the structure of the optimal electrolyte. The SiO_2 nanoparticles are surrounded by AIIP chains through formation of hydrogen bonds. Then, the AIIP chains are further surrounded by chains of I^- and I_3^- through electrostatic interactions, thus constructing highly-efficient electron exchange tunnels. The corresponding device using a triphenylamine-based metal-free organic dye (TC15) exhibited conversion efficiencies of 2.70 and 4.12% under the illumination of 100 and 10 mW cm^{-2}, respectively. A single wall carbon nanotube (SWCNT)-based binary IL electrolyte ([EMIM]I : [PMIM]I = 40 : 60, weight ratio) exhibited an efficiency of 3.49%, as well as excellent durability compared with that of traditional liquid electrolytes.[222] Especially, the SWCNTs acted as both a filler for the physical gelation of the electrolyte and a catalyst for the reduction of I_3^-. Ccomposite electrolytes with different contents of carbon black in [PMIM]I were also reported by Lei *et al.*[223] The photovoltaic performance of the DSC was found to strongly depend on the carbon black content and the TiO_2 film thickness. The highest conversion efficiency of 6.37% was achieved with the electrolyte composition of 100 mg [PMIM]I and 60 mg carbon black, and a 16.2 μm TiO_2 film. The solid device based on an electrolyte composed of PVPPEGMEI and I_2, combined with a SWCNT counter electrode and N621 dye, achieved a conversion efficiency of 3.7% under 100 mW cm^{-2} illumination.[224]

An I_2-free solid-state DSC based on PEBII and PVC-*g*-POEM-directed TiO_2 film obtained an efficiency of 5.93% at 100 mW cm^{-2}.[225] The superior photovoltaic performance was attributed to the improved interfacial properties of the electrode/electrolyte and the enhanced electron lifetime. Subsequently, the efficiency of the cell was further improved to 7.1%.[226] Another series of IL polymers, PAAII, were also applied as I_2-free solid-state electrolytes.[227] Among them, PEAII exhibited the highest efficiency of 5.29% under illumination of 100 mW cm^{-2}. Instead of improving the photovoltaic performance of the device, introducing I_2 into the electrolyte system resulted in a negative effect. This can be analyzed as a result of the enhanced recombination of injected electrons with polyiodides, increased dark current and light absorption caused by the polyiodides.

Carbazole-imidazolium (CBZ-IMDZ)-structured solid state ionic conductors were synthesized and applied for DSCs.[228] The device based on this electrolyte (0.12 M methyl substituted carbazole-imidazolium iodide, 0.03 M I_2, 0.1 M TBP, 0.12 M Li[TFSI] and 0.012 M [EMIM][BF_4]) obtained an efficiency of 2.85% with a diffusion coefficient of 2.2×10^{-7} for I_3^-. The operating mechanism was interpreted as follows. The iodide was firstly oxidized by regenerating the oxidized dye. The formed iodine radical was then reduced to iodide by the CBZ-IMDZ cation. The hole in CBZ-IMDZ can be transported by a hopping mechanism to the counter electrode. Furthermore, the CBZ can also assist the transport of the iodine radical. Other ester-functionalized ionic conductors based on the imidazolium cation and iodide anion were developed by Wang's group (Fig. 38).[229] The effect of the substituent group was systematically investigated. The ester-functionalized methyl-imidazolium iodide electrolyte showed a superior conductivity

Table 4 Quasi-solid-state electrolytes for DSCs

Authors	Electrolytes	Light intensity (mW cm^{-2})	Dye	V_{oc} (mV)	J_{sc} (mA cm^{-2})	FF	η (%)	Ref.
Wang *et al.*	5 wt% SiO_2, 0.5 M I_2, 0.45 M NMBI in pure [PMIM]I	99.2	Z907	672	12.75	0.709	6.1	210
Cheng *et al.*	1 wt% α-TiP, 0.15 M I_2, 0.1 M GuSCN, 0.5 M TBP in [PMIM]I/[EMIM][BF_4] (13 : 7, volume ratio)	100	N3	679	17.212	0.518	6.05	211
Chen *et al.*	11.1 wt% PACB, 0.05 M I_2, 0.1 M LiI, 0.5 M TBP in [EMIM][SCN]/[PMIM]I (35 : 65, volume ratio)	100	N719	760	11.2	0.72	6.15	212
Jin *et al.*	TPC/IL electrolyte (5 : 1, volume ratio), IL electrolyte: 0.05 M I_2, 0.1 M LiI and 0.45 M NMBI in MPN/[PMIM]I (1 : 2, volume ratio)	100	N3	628	13.87	0.74	6.45	213
Wang *et al.*	10 wt% precursors (PPDD : DHD = 1 : 2, molar ratio), 0.1 M LiI, 0.5 M I_2, 0.5 M NMBI in HMII/MPN (13 : 7, volume ratio)	100	N3	700	13.67	0.73	7.00	214
Wang *et al.*	10 wt% P([MOEMIM]Cl), 0.5 M I_2, 1 M LiI, 0.5 M NMBI in [HMIM]I/[EMIM][BF_4] (2 : 1, weight ratio)	100	N3	618	15.50	0.64	6.1	215
Sun *et al.*	1 wt% DMBS, 0.05 M I_2, 0.5 M LiI, 0.4 M [DMPIM]I), 0.5 M TBP in [EMIM][BF_4]	100	N719	740	6.59	0.75	3.63	216
Qin *et al.*	PHDDA/[HMIM]I/PEGDME (1 : 4.8 : 3.2, weight ratio) with 10 μL of I_2-TBP solution (0.3 M)	100	N719	671	12.1	0.719	5.83	217
Fang *et al.*	20 wt% PH-I, [HMIM]I, [AMIM]I, NMBI, GNCS (8 : 8 : 1.2 : 1.2, molar ratio)	100	N3	643	15.10	0.72	6.95	218
Zhao *et al.*	25 wt% [PBVIm][TFSI], 0.1 M I_2, 0.1 M LiI, 0.5 M TBP in [PMIM]I/[EMIM][TFSI] (13 : 7, volume ratio)	100	N3	613	10.57	0.678	4.4	219
Chen *et al.*	25 wt% [PBVIM][TFSI], 15 wt% of IL–TiO_2 nanoparticles, 0.1 M I_2, 0.5 M TBP, 0.1 M GNCS, [EMIM]I/[PMIM]I/[EMIM][SCN] (6 : 6 : 7, volume ratio),	100	N3	659	11.66	0.683	5.26	220

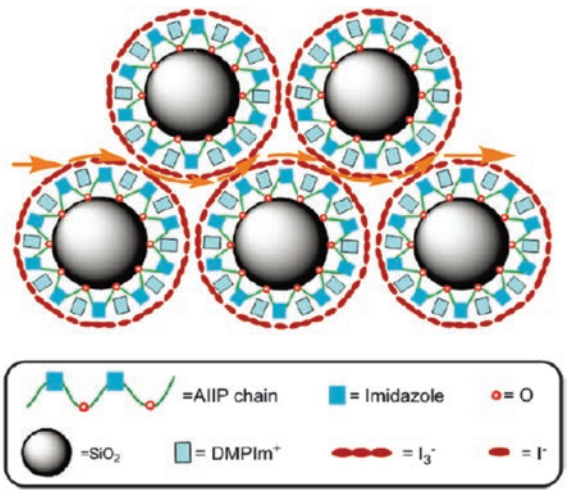

Fig. 37 Schematic structure of the composite electrolyte containing AIIP, SiO_2, I_2, and [DMPIM]I. Reprinted with permission from ref. 221.

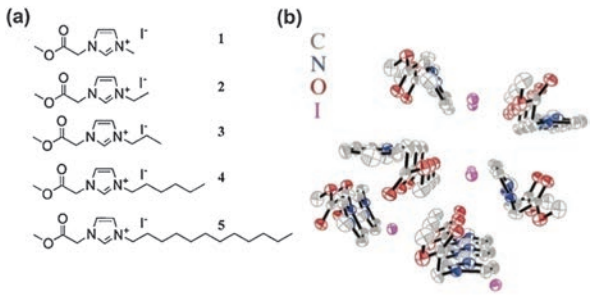

Fig. 38 (a) Structures of the ester-functionalized ionic conductors. (b) The crystallographic packing structure of conductor 1. Adapted with permission from ref. 229.

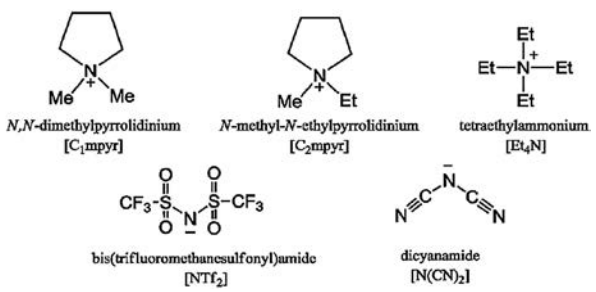

Fig. 39 Structures of the cations and anions in organic ionic plastic crystals. Reprinted with permission from ref. 230.

of 5.76 mS cm^{-1} and the highest conversion efficiency of 6.63%. The high conductivity was attributed to the formation of three-dimensional ionic channels and the interaction of Li^+ with the oxygen in the ester group, which resulted in fast charge transfer. The good long-term stability was demonstrated as the efficiency remained at 100% of the initial value after 1000 h.

Organic ionic plastic crystals (OIPCs) are a new class of electrolyte. As shown in Fig. 39, Pringle's group reported a series of OIPC electrolytes for solid DSCs. The highest conversion efficiency of 5.1% was achieved based on [C_1mpyr][$N(CN)_2$], which was consistent with the superior diffusion coefficient of 6.2×10^{-7} cm^2 s^{-1}.[230] However, the results showed that the photovoltaic performance of the DSC is not dependent solely on factors such as conductivity or diffusivity. Electrolytes based on $P_{12}I$ (35 wt% [PMIM]I doped $P_{12}I$ and 0.2 M I_2) were also developed.[231] The high diffusion coefficient for I^- and I_3^- in the solid electrolyte were determined as 0.43×10^{-6} and 0.39×10^{-6} cm^2 s^{-1} at 25 °C, respectively. Such high ion diffusivity was attributed to the decoupling of rotational

Table 5 Solid-state electrolytes for DSCs

Authors	Electrolytes	Light intensity (mW cm^{-2})	Dye	V_{oc} (mV)	J_{sc} (mA cm^{-2})	FF	η (%)	Ref.
Shi *et al.*	I_2 (with a mole ratio of I_2/O = 0.9), [DMPIM]I (with a mole ratio of [DMPIM]I/O = 0.6), 1 wt% SiO_2 in AIIP	100	TC15	619	7.80	0.560	2.70	221
Lee *et al.*	SWCNTs : [EMIM]I/[PMIM]I (40 : 60, weight ratio) (1 : 9, weight ratio)	100	N719	716	7.07	0.61	3.49	222
Lei *et al.*	100 mg [PMIM]I, 60 mg carbon black	100	N719	644	15.33	0.645	6.37	223
Kawano *et al.*	PVPPEGMEI/I_2([I^-] : [I_2] = 4 : 1)	100	N621	700	9.0	0.58	3.7	224
Chi *et al.*	PEBII	100	N719	643	18.1	0.51	5.93	225
Ahn *et al.*	PEBII	100	N719	840	13.8	0.61	7.1	226
Wang *et al.*	PEAII	100	N3	838	9.75	0.65	5.29	227
Midya *et al.*	0.12 M methyl substituted [CBZ-IMDZ]I, 0.03 M I_2, 0.1 M TBP, 0.12 M Li[TFSI], 0.012 M [EMIM][BF_4]	100	N719	718	6.23	0.637	2.85	228
Wang *et al.*	Ester-functionalized [MIM]I with I_2 and LiI (5 : 1 : 1.25, molar ratio)	100	MK-2	660	13.77	0.73	6.63	229
Armel *et al.*	2.50 M [C_2mim][I], 0.1 M LiI, 0.23 M I_2, 0.25 M NMBI in [C_1mpyr][$N(CN)_2$]	100	N719	775	8.6	0.77	5.1	230
Li *et al.*	35 wt% [PMIM]I doped $P_{12}I$, 0.2 M I_2	100 (80 °C)	Z907	609	12.44	0.685	5.20	231

disorder, the existence of vacancies in the lattice and the Grotthus electron-exchange mechanism. A high efficiency of 5.2% was obtained at 80 °C under irradiation of 100 mW cm^{-2}, while the corresponding value was 4.85% at room temperature. Table 5 summarizes the detailed information.

4.2 Energy storage

4.2.1 Lithium-ion batteries. The large scale application of lithium-ion batteries is greatly hindered by the safety problems resulting from conventional organic electrolytes, such as the greatly increased internal pressure of the device due to the poor stability and decomposition of organic solvents under overheating or overpotentials, the inflammable property, and the leakage of electrolyte due to its volatile nature. To solve this well known challenge, IL alternatives are attractive for developing safe, non-flammable devices with wide temperature ranges.

The imidazolium family is the most commonly used for the IL electrolyte of lithium-ion batteries. An electrolyte containing [EMIM][FSI] with 0.3 mol kg^{-1} LiTFSI was applied to a Si–Ni–C composite anode in lithium-ion batteries.[232] The galvanostatic cycling of FSI-based electrolyte with the composite anode resulted in a charge limitation of 800 mA h g^{-1} and a discharge capacity of 790 mA h g^{-1} even at the 50th cycle, whereas the common IL electrolyte with the TFSI anion showed no reversible capacity to the anode. This result can be ascribed to the low interfacial and charge transfer resistances at the anode for the FSI-based electrolyte. The bicyclic imidazolium IL [ETMIM][TFSI] was found to not only increase the reduction stability of pure IL but also improve the electrochemical performance of the electrolyte in a Li‖graphite half-cell.[233] Reversible capacities of 250 mA h g^{-1} and 70 mA h g^{-1} at 25 °C, and 330 mA h g^{-1} and 250 mA h g^{-1} at 50 °C, were achieved under current rates of C/20 and C/10, respectively.

Besides the imidazolium family, other types of ILs have also been investigated. Sakaguchi's group reported an IL electrolyte consisting of [$MEMBu_3P$][TFSI] for lithium-ion batteries with Si thick-film electrodes.[234] An initial discharge capacity of 3450 mA h g^{-1} and a coulombic efficiency of 86% were achieved with [$MEMBu_3P$][TFSI]. For comparison, the commonly used IL [PP13][TFSI] gave the corresponding values of 1900 mA h g^{-1} and 85%, and the related values for propylene carbonate (PC) were 3390 mA h g^{-1} and 78%. The excellent performance of [$MEMBu_3P$][TFSI] was attributed to the effective suppression of electrode collapse and the electrical isolation induced by the pulverization during the charge–discharge cycling, as well as the more effective desolvation of Li ions from the anions when compared with PC. The four ILs with the cations of [PP13] or [EMIM] and anions of [FSI] or [TFSI] were combined with a $LaSi_2$–Si composite anode.[235] The [PP13][FSI] exhibited the best performance, and was even better than the conventional organic PC electrolyte. Discharge capacities of 1000 mA h g^{-1} and 800 mA h g^{-1} were obtained at the first cycle and the 250th cycle, respectively. This result can be ascribed to the smoother Li ion transfer, and the easier desolvation of Li ions and [FSI] anions at the electrode/electrolyte interface, as well as the higher stability of [PP13] cations against cathodic decomposition. To achieve a greener and safer device, CarboxyMethylCellulose (CMC) was used as a binder for both the anodic ($Li_4Ti_5O_{12}$) and cathodic active materials ($LiFePO_4$) of a lithium-ion battery with [PYR_{14}][FSI] electrolyte.[236] The device realized a discharge capacity of about 140 mA h g^{-1} with a charge efficiency higher than 99% for 160 cycles. The [PYR_{14}][TFSI] and graphite composite anode exhibited high electrochemical stability, capacity (350–360 mA h g^{-1}) and cycling efficiency (99.5–99.8%) within 50 cycles.[237]

To investigate the microscopic processes in batteries, Huang *et al.* reported a nanoscale electrochemical device consisting of a single SnO_2 nanowire anode, IL electrolyte, and a $LiCoO_2$ cathode to realize the real-time observation of the lithiation of SnO_2 nanowire during electrochemical charging.[238] As shown in Fig. 40, when a potential of −3.5 V *vs.* $LiCoO_2$ was applied, the reaction propagated along the longitudinal direction of the nanowire, causing the nanowire to elongate, swell, and spiral. The time for charging the nanowire (length: 16 mm and

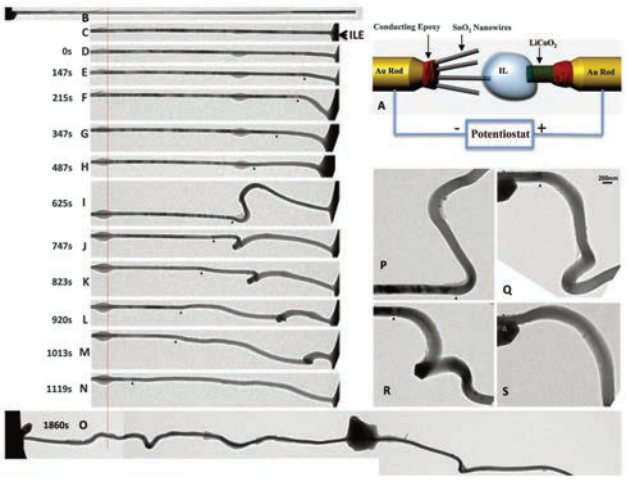

Fig. 40 Structure evolution of a SnO_2 nanowire anode during charging. (A) Schematic of the electrochemical device. The initially straight nanowire (B and C) became significantly twisted and bent after charging (D to S). Adapted with permission from ref. 238.

diameter: 188 nm) was about half an hour. The generation and migration of the dislocations near the reacting interface shown in Fig. 41 gave proof that the dislocations were continuously nucleated in the crystal regions and then moved away from the highly stressed region. The observed high density of the observed dislocations (with the order of 10^{17} m^{-2}) was caused by the exceptionally high stress driven from the electrochemical reaction. These dislocations may be effective channels for Li transport and facilitate the insertion of Li ions into the crystalline interior, thus increasing the reaction kinetics. The obtained results clarified the mechanisms determining the performance of the battery with the microstructure.

A soft matter polymer gel electrolyte was obtained by free radical polymerization of acrylonitrile in IL electrolyte (LiTFSI, $[Py_{1,4}][TFSI]$), as shown in Fig. 42.[239] This gel electrolyte can be used in $LiFePO_4$ cells without a separator. With a similar ionic conductivity and stability to the IL, the IL-based gel electrolyte exhibited superior cyclability and rate capability to the IL, which could be attributed to the multifunctional role of the gel material, such as the ion conductor and separator. The solid-state electrolyte with LiSICON-IL ($[PYR_{13}][FSI]$) was investigated at temperatures from 25 °C to 120 °C.[240] The cell with

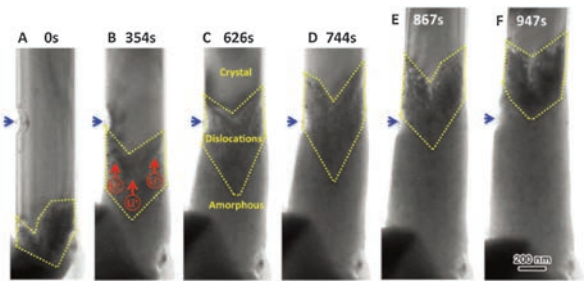

Fig. 41 TEM images (A to F) of the dislocations at different times. Adapted with permission from ref. 238.

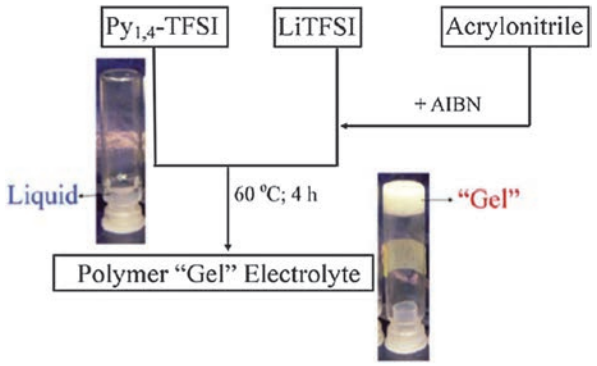

Fig. 42 Schematic diagram for the synthesis of polymer gel electrolyte. Reprinted with permission from ref. 239.

0.75 M LiTFSI/$[PYR_{13}][FSI]$ achieved a capacity of 310 mA h g^{-1} and a coulombic efficiency of 99.8% during cycling at 80 °C.

4.2.2 Supercapacitors. As one kind of important energy storage device, supercapacitors, including electric double-layer capacitors (EDLCs) and pseudocapacitors, have attracted increasing attention for broad applications due to their advantages of high power density, long cycle life, maintenance-free operation, simple charging circuit and lack of memory effect. Considering the main drawback of low breaking-up voltage (<1.0 V) based on the traditional aqueous electrolytes, ILs are regarded as potential alternatives with a larger window of stability.

Fluorohydrogenate ILs (FHILs) with different cations were developed as the electrolytes for EDLCs with carbon electrodes. The FHILs exhibited higher capacitances than $[EMIM][BF_4]$ and $[TEA][BF_4]$/PC in the voltage range from 1.0 to 3.2 V. The maximum capacitance was found to be inverse to the size of the cation, and the highest capacitance of 178 F g^{-1} was obtained for $[DMIM][(FH)_{2.3}F]$. This attractive result showed high capacitance even at the low temperature of −40 °C for the FHILs.[241] The effects of the anion composition and the size of [EMIM]-based ILs on the Bi(111) electrode/IL interface in EDLCs were also investigated.[242] Among the anions of tris(pentafluoroethyl) trifluorophosphate ($[FAP]^-$), $[TCB]^-$ and $[BF_4]^-$, $[FAP]^-$ exhibited the lowest series capacitance value due to its biggest diameter and closest approach of the mass centre to the electrode surface. Liu *et al.* reported a supercapacitor with an $[EMIM][BF_4]$-based electrolyte and a graphene electrode.[243] As shown in Fig. 43, the excellent capacitance of the graphene electrode, and the $[EMIM][BF_4]$-based electrolyte capable of operating at a high voltage of 4 V, results in energy densities of 85.6 W h kg^{-1} at room temperature and 136 W h kg^{-1} at 80 °C at 1 A g^{-1}, which is one of the highest values ever reported using carbon electrodes without pseudocapacitance contributions from a conducting polymer or metal oxide. Polypyrrole-derived activated carbon combined with $[EMIM][BF_4]$ electrolyte in an EDLC achieved a specific capacitance of 300 F g^{-1}, which is a more than two-fold improvement compared to commercial carbons.[244] The charge–discharge test at 60 °C showed that there was no visible degradation for the

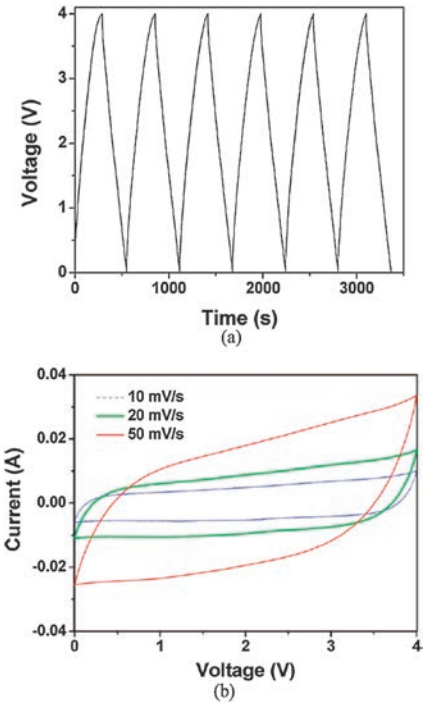

Fig. 43 (a) Galvanostatic charge–discharge curve of the graphene electrode at a constant current density of 1 A g^{-1}, using [EMIM][BF_4] electrolyte. (b) Cyclic voltammograms of the graphene electrode with [EMIM][BF_4] IL electrolyte at different scan rates. Reprinted with permission from ref. 243.

assembled EDLC after 10 000 galvanostatic cycles. A supercapacitor consisting of [Bu_3HP][BF_4]/acetonitrile electrolyte and a carbon anode was also developed.[245] The corresponding device exhibited a large electrochemical window of about 6 V, an operating voltage of 1.5 V, a comparable capacity to conventional aqueous electrolyte, stable cycling abilities and a wide operating temperature, ranging from −40 °C to 80 °C, which showed the promising application of [Bu_3HP][BF_4] in electrolyte.

To achieve an IL-compatible graphene-based electrode, poly(IL) was introduced for surface modification of the electrode to enhance the effective surface area of the electrode/electrolyte interface.[246] The obtained poly(IL)-modified reduced graphene oxide exhibited enhanced compatibility with [EMIM][TFSI] electrolyte. The corresponding supercapacitor achieved a stable electrochemical response (operating voltage of 3.5 V), a maximum energy density of 6.5 W h kg^{-1} and a maximum power density of 2.4 kW kg^{-1}.

Thereafter, at the molecular level, a supercapacitor composed of nanoporous carbon and [EMIM][BF_4] electrolyte was investigated by computer simulation.[247] The molecular dynamics (MD) simulation result showed that the pore size of the carbon has a significant effect on the distribution of IL inside the micropores. As shown in Fig. 44, a well-defined single-file distribution at the axis, a zigzag structure, a discernible co-ion structure and three internal solvation shell-distributions were assigned to the (6, 6), (8, 8), (10, 10), and (15, 15) nanotubes (with diameters of 0.81, 1.08, 1.35 and 2.03 nm), respectively. The capacitance of the carbon nanotubes increased with decreasing the diameter in the range of 0.9–2 nm, due to the more important role that internal counterions play with smaller micropore diameters. However, the lack of internal solvation caused a rapid drop in the capacitance when reducing the diameter below ~0.8 nm. The above result was in accordance with experiments. This will provide guidance for understanding the effects of electrode geometry on specific capacitance and power efficiency at the molecular level.

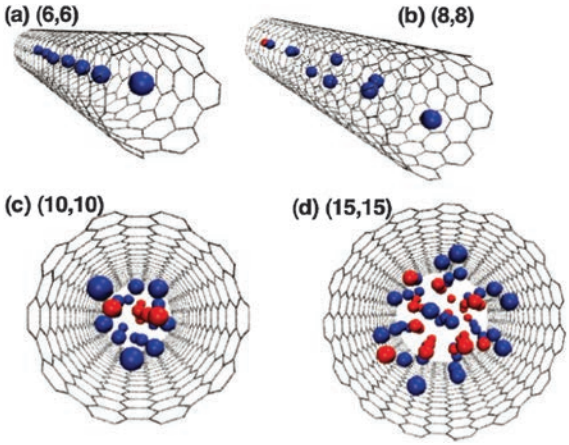

Fig. 44 The distributions of IL ions inside CNT anodes. The red and blue dots represent the center-of-mass positions of $[EMIM]^+$ and $[BF_4]^-$, respectively. Reprinted with permission from ref. 247.

Kim's group reported a series of work on all-solid-state flexible supercapacitors.[248,249] The devices (Fig. 45) were developed by coating CNTs onto office paper, and combining with [EMIM][TFSI]/silica electrolyte.[248] The IL-based electrolyte exhibited a superior capacitance of 135 F g^{-1}, a maximum power of 164 kW kg^{-1}, and an energy density of 41 W h kg^{-1}, which was comparable to that of the IL electrolyte. The excellent stability was confirmed over 4000 charge–discharge cycles, with a variation of less than 3% in the specific capacitance. Subsequently, a gel electrolyte based on [EMIM][TFSI] and polymer (PSPEO-PS) was investigated with CNT/bacterial nanocellulose paper.[249] The supercapacitor exhibited a specific capacitance of 50.5 F g^{-1}, an energy of 15.5 mW h g^{-1}, and a power of 1.5 W g^{-1}. Over 5000 charge–discharge cycles there was a less than 0.5% change in the specific capacitance, giving direct proof of the excellent stability of the device.

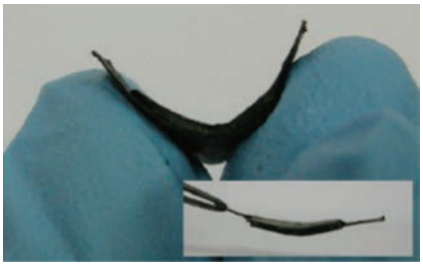

Fig. 45 Photograph of the flexible supercapacitor (inset: before bending). Adapted with permission from ref. 248.

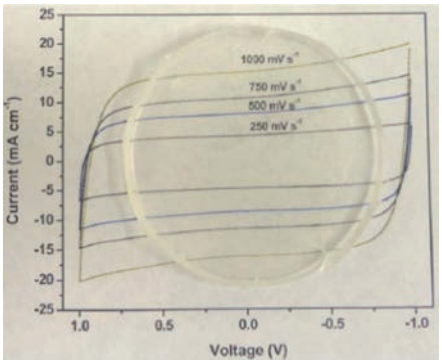

Fig. 46 Photograph of the transparent gel polymer electrolyte film. Reprinted with permission from ref. 250.

Other types of electrolytes have also been investigated. A gel electrolyte based on [EMIM][TCB] and PVdF-HFP has been prepared as shown in Fig. 46.[250] With excellent thermal stability up to 310 °C, an electrochemical window of 3.8 V and a high ionic conductivity of 9×10^{-3} S cm^{-1} at room temperature, the corresponding EDLC showed a capacitance of 34.4 F g^{-1}, comparable to the value of 37.3 F g^{-1} for the pure IL-based device. A plastic crystal IL, [Me_3S][TFSI], was also developed.[251] With electrochemical and thermal stability, high conductivity, and a large electrochemical window of around 5 V, the corresponding device resulted in a good capacitance of 150 F g^{-1}, indicating the potential of [Me_3S][TFSI] as the electrolyte of supercapacitors.

4.2.3 Lithium–air (O_2) batteries. Due to their high theoretical energy density, lithium–air (O_2) batteries have been attracting intensive attention.[252,253] To overcome the drawbacks and limitations of traditional liquid electrolytes, IL-based electrolytes have been reported recently. Zhou's research group chose [EMIM][TFSI] combined with SWNTs to form a cross-linked network gel (CNG) for the oxygen electrode (Fig. 47).[252] Different from the conventional three-phase electrochemical interface, the SWNT–IL CNG system was demonstrated to allow the three-dimensional tricontinuous passage of electrons, ions, and oxygen by expanding the three-phase reactive interface to the whole cross-linked network, thus improving the performance of the device. A specific energy density of 2440 W h kg^{-1}, a specific power density of 1660 W kg^{-1} and a reversible discharge–charge capacity of 10 730 mA h g^{-1} in ambient air were achieved. The results showed the possibility of moving from lithium–O_2 batteries to lithium–air batteries with the developed CNG. A [EMIM][BF_4]-based electrolyte coupled with γ-MnOOH nanorods/carbon has also demonstrated an effective influence on improving the performance of lithium–O_2 batteries.[254] The corresponding device exhibited a high discharge capacity of 9400 mA h g^{-1} at a current density of 50 mA g^{-1} and 100-cycle stability with a current density of 200 mA g^{-1}, which can be ascribed to the O_2-stability and wide electrochemical potential window of the IL-based electrolyte.

A polymer composite electrolyte composed of [DMPIM][TFSI], silica and PVdF-HFP was developed for lithium–air batteries.[253] The discharge capacity for the carbon-catalyzed battery was 2800 mA h g^{-1}, which is higher than the value of 1500 mA h g^{-1} for the pure IL electrolyte. The α-MnO_2-catalyzed cell exhibited an extended initial discharge capacity of 4080 mA h g^{-1} of carbon, which was 2040 mA h g^{-1} associated with the total mass of the cathode.

4.2.4 Vanadium redox flow batteries. As a new kind of electrochemical device for energy storage, vanadium redox flow batteries (VRBs, Fig. 48) are regarded as important and promising technology.[255,256] The traditional aqueous electrolytes resulted in a limited operating potential and low energy

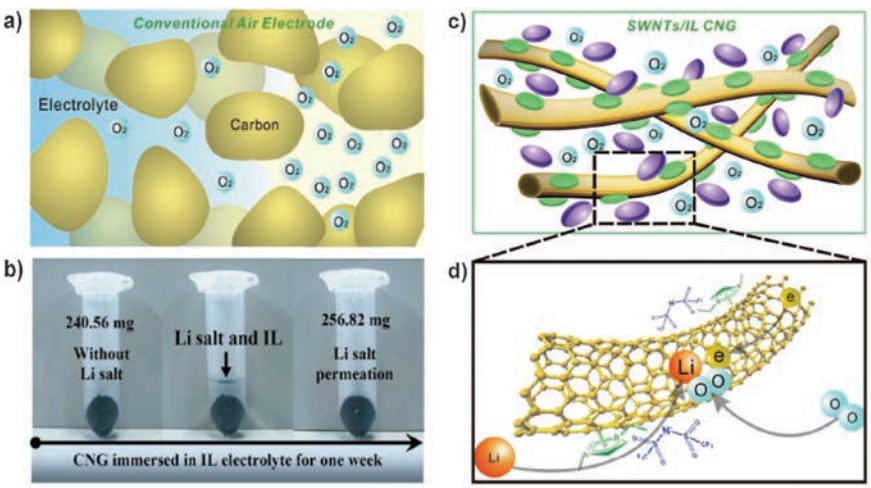

Fig. 47 Schematic representations comparing the conventional air electrode with the CNG air electrode. (a) The air electrode using a conventional carbonaceous material. (b) The weight variation of the CNG after immersion in IL electrolyte for one week. (c) CNG. (d) Three dimensional tricontinuous passage of electrons, ions, and oxygen. Electrons conduct along the carbon nanotubes. Li ions are transferred from the IL electrolyte outside into the CNG and are coordinated by the inside-anchored $[NTf_2]^-$. Oxygen in the CNG incorporates with the Li ions and the electrons along the SWNTs, thereby turning into the discharge products. Reprinted with permission from ref. 252.

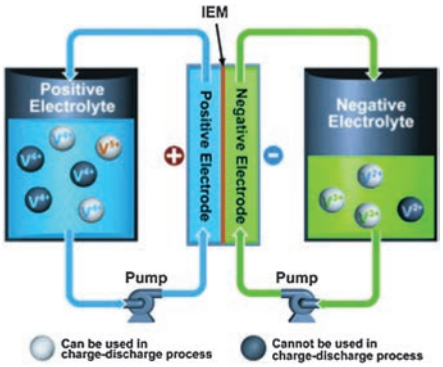

Fig. 48 Schematic illustration of a vanadium redox flow battery. Reprinted with permission from ref. 255.

density.[257] To acquire a higher operating potential window, and excellent energy and power densities, a non-aqueous device is highly needed. Li *et al.* reported a non-aqueous VRB with [TEA][PF_6] and [EMIM][PF_6] as electrolytes, and vanadium acetylacetonate ($V(acac)_3$) as the active species.[257] The two ILs are stable in the operating potential range from −2.5 to 1.5 V. The conductivity of the electrolytes and the diffusion coefficient of the active species ($V(acac)_3$) increased with increasing the concentration of the ILs. The diffusion coefficients of $V(acac)_3$ were 0.92–1.47 × 10^{-6} cm^2 s^{-1} in 0.5 M [TEA][PF_6] and 2.35–3.79 × 10^{-6} cm^2 s^{-1} in [EMIM][PF_6]. The [TEA][PF_6] (0.2 M) electrolyte showed coulombic efficiencies of 53.31% for the 3rd cycle and 57.44% for the 4th cycle at a 50% state of charge, respectively, which were higher than the corresponding values of 46.04 and 43.46% for the [EMIM][PF_6]-based electrolyte.

5. Conclusions and prospects

Serious energy and environmental problems have stimulated rapid growth in exploring renewable energy produced from CO_2, biomass and solar energy. This review indicates the great potential application of ILs in renewable energy production, with virtues including high efficiency and superior stability. However, this field is in its infancy and a number of issues need to be investigated in the future.

CO_2 is an inert chemical, thus, its activation generally causes high energy input and cost. In addition, it is highly expected that flue gas will be used as a raw material in order to reduce cost. The corresponding critical reaction conditions caused by the nature of the reaction and the raw materials might be the primary obstacles limiting the substitution of traditional energy production catalysts with ILs. As a result, the development of highly stable and efficient ILs is required to realize the large scale application of ILs. Further related work is suggested to deeply study the mechanisms of the reactions, to design functional ILs, and to explore new routes for the production of fuels and fuel additives from CO_2 based on ILs.

In the dissolution and conversion of biomass, the formation of hydrogen bonds between the ILs and the cellulose hydroxyl groups is the key factor in breaking the inter- and intramolecular hydrogen bonds of the biomass. The synergistic interactions of anions and cations with the cellulose hydroxyl groups lead to the dissolution of cellulose in ILs. ILs also serve as good solvents and catalysts for the conversion of cellulose and lignin. Most of the current systems for the dissolution and conversion of biomass require relatively high temperatures (>100 °C) and a long time. From the viewpoint of energy conservation and cost saving, processes operated at low temperatures with low cost ILs still need to be explored.

In photoelectric conversion processes, IL-based electrolytes with excellent long-term stability exhibit the foreseeable future for the outdoor use of DSCs. To further improve the conversion efficiency and realize the actual commercial application, a deep understanding of the specific interaction mechanism of the IL electrolyte and the factors that affect the photovoltaic performance of the device is still needed. Attractive work can be expected by developing low viscosity ILs, new families of IL-based electrolytes and the corresponding adapted dyes, as well as electrode materials to overcome the restrictions and fully explore the potential of IL electrolytes. In the case of energy storage devices, there are still some aspects that need to be further improved, such as the development of ILs with excellent low temperature performance, the systematic investigation of the relationship between ILs and the performance of devices, and the mechanism of the IL/electrode interface.

Based on the above discussions, future work is suggested to focus on the following aspects:

(i) Fully and deeply master the structure–property relationship of ILs by a combination of experiments and simulation methods for designing new kinds of ILs with low viscosity, high stability and activity, and low cost.

(ii) Explore the corresponding effective methods for separation and recovery of ILs with low energy consumption.

(iii) Develop large scale integrated processes for producing renewable energy and chemicals from CO_2, biomass and solar power.

Although some issues still exist in IL application, we believe that green processes and innovative energy producing technology based on ILs will be highly expected with persistent effort and continuous attention.

Acknowledgements

The authors acknowledge the financial support provided by the National Natural Science Foundation of China (No. 21210006, 21127011, 21106146, 21006117, 51203161, 21006112 and 21276260).

References

1 E. G. Pereira, J. N. da Silva, J. L. de Oliveira and C. S. Machado, *Renewable Sustainable Energy Rev.*, 2012, **16**, 4753–4762.
2 P. J. Dunn, *Chem. Soc. Rev.*, 2012, **41**, 1452–1461.

3 R. A. Sheldon, *Chem. Soc. Rev.*, 2012, **41**, 1437–1451.
4 V. I. Pârvulescu and C. Hardacre, *Chem. Rev.*, 2007, **107**, 2615–2665.
5 F. V. Rantwijk and R. A. Sheldon, *Chem. Rev.*, 2007, **107**, 2757–2785.
6 N. V. Plechkova and K. R. Seddon, *Chem. Soc. Rev.*, 2008, **37**, 123–150.
7 M. Petkovic, K. R. Seddon, L. P. N. Rebelo and C. Silva Pereira, *Chem. Soc. Rev.*, 2011, **40**, 1383–1403.
8 C. Maton, N. De Vos and C. V. Stevens, *Chem. Soc. Rev.*, 2013, **42**, 5963–5977.
9 X. B. Lu and D. J. Darensbourg, *Chem. Soc. Rev.*, 2012, **41**, 1462–1484.
10 T. Erdmenger, C. Guerrero-Sanchez, J. Vitz, R. Hoogenboom and U. S. Schubert, *Chem. Soc. Rev.*, 2010, **39**, 3317–3333.
11 T. L. Greaves and C. J. Drummond, *Chem. Soc. Rev.*, 2013, **42**, 1096–1120.
12 S. N. Riduan and Y. Zhang, *Chem. Soc. Rev.*, 2013, **42**, 9055–9070.
13 X. Zhang, X. Zhang, H. Dong, Z. Zhao, S. Zhang and Y. Huang, *Energy Environ. Sci.*, 2012, **5**, 6668–6681.
14 C. Song, *Catal. Today*, 2006, **115**, 2–32.
15 S. Sankaranarayanan and K. Srinivasan, *Indian J. Chem.*, 2012, **51A**, 1252–1262.
16 D. M. Alonso, J. Q. Bond and J. A. Dumesic, *Green Chem.*, 2010, **12**, 1493–1513.
17 A. M. Lakaniemi, O. H. Tuovinen and J. A. Puhakka, *Bioresour. Technol.*, 2013, **135**, 222–231.
18 R. C. Baliban, J. A. Elia and C. A. Floudas, *Ind. Eng. Chem. Res.*, 2013, **52**, 3381–3406.
19 M. J. Bussemaker and D. Zhang, *Ind. Eng. Chem. Res.*, 2013, **52**, 3563–3580.
20 R. M. Navarro, M. A. Peña and J. L. G. Fierro, *Chem. Rev.*, 2007, **107**, 3952–3991.
21 T. R. Cook, D. K. Dogutan, S. Y. Reece, Y. Surendranath, T. S. Teets and D. G. Nocera, *Chem. Rev.*, 2010, **110**, 6474–6502.
22 Y. Hou, R. Vidu and P. Stroeve, *Ind. Eng. Chem. Res.*, 2011, **50**, 8954–8964.
23 D. C. Hoppock and D. Patino-Echeverri, *Environ. Sci. Technol.*, 2010, **44**, 8758–8765.
24 B. J. Mincher, *ACS Symp. Ser.*, 2010, **1046**, 3–10.
25 T. W. Hamann and J. W. Ondersma, *Energy Environ. Sci.*, 2011, **4**, 370–381.
26 M. Wang, C. Gratzel, S. M. Zakeeruddin and M. Gratzel, *Energy Environ. Sci.*, 2012, **5**, 9394–9405.
27 M. Mikkelsen, M. Jørgensen and F. C. Krebs, *Energy Environ. Sci.*, 2010, **3**, 43–81.
28 T. Sakakura, J. C. Choi and H. Yasuda, *Chem. Rev.*, 2007, **107**, 2365–2387.
29 W. Wang, S. Wang, X. Ma and J. Gong, *Chem. Soc. Rev.*, 2011, **40**, 3703–3727.
30 K. I. Tominaga, Y. Sasaki, K. Hagihara, T. Watanabe and M. Saito, *Chem. Lett.*, 1994, 1391–1394.
31 L. C. Wang, M. Tahvildar Khazaneh, D. Widmann and R. J. Behm, *J. Catal.*, 2013, **302**, 20–30.
32 L. Wang, H. Liu, Y. Liu, Y. Chen and S. Yang, *J. Rare Earths*, 2013, **31**, 559–564.
33 S. S. Kim, H. H. Lee and S. C. Hong, *Appl. Catal., B*, 2012, **119–120**, 100–108.
34 S. S. Kim, H. H. Lee and S. C. Hong, *Appl. Catal., A*, 2012, **423–424**, 100–107.
35 G. Zhao, T. Jiang, B. Han, Z. Li, J. Zhang, Z. Liu, J. He and W. Wu, *J. Supercrit. Fluids*, 2004, **32**, 287–291.
36 J. O. M. Bockris and J. C. Wass, *J. Electrochem. Soc.*, 1989, **136**, 2521–2528.
37 K. Chandrasekaran and L. O. M. Bockris, *Surf. Sci.*, 1987, **185**, 495–514.
38 B. A. Rosen, A. Salehi-Khojin, M. R. Thorson, W. Zhu, D. T. Whipple, P. J. Kenis and R. I. Masel, *Science*, 2011, **334**, 643–644.
39 B. A. Rosen, J. L. Haan, P. Mukherjee, B. Braunschweig, W. Zhu, A. Salehi-Khojin, D. D. Dlott and R. I. Masel, *J. Phys. Chem. C*, 2012, **116**, 15307–15312.
40 B. A. Rosen, W. Zhu, G. Kaul, A. Salehi-Khojin and R. I. Masel, *J. Electrochem. Soc.*, 2013, **160**, H138–H141.
41 J. Lin, Z. Ding, Y. Hou and X. Wang, *Sci. Rep.*, 2013, **3**, DOI: 101038/srep01056.
42 W. Reutemann and H. Kieczka, Wiley-VCH, Weinheim, 2009.
43 S. Enthaler, J. von Langermann and T. Schmidt, *Energy Environ. Sci.*, 2010, **3**, 1207–1217.
44 C. Fellay, P. J. Dyson and G. Laurenczy, *Angew. Chem., Int. Ed.*, 2008, **47**, 3966–3968.
45 B. Loges, A. Boddien, H. Junge and M. Beller, *Angew. Chem., Int. Ed.*, 2008, **47**, 3962–3965.
46 A. Boddien, F. Gartner, C. Federsel, P. Sponholz, D. Mellmann, R. Jackstell, H. Junge and M. Beller, *Angew. Chem., Int. Ed.*, 2011, **50**, 6411–6414.
47 A. Boddien, B. R. Loges, F. Gärtner, C. Torborg, K. Fumino, H. Junge, R. Ludwig and M. Beller, *J. Am. Chem. Soc.*, 2010, **132**, 8924–8934.
48 B. Kumar, M. Llorente, J. Froehlich, T. Dang, A. Sathrum and C. P. Kubiak, *Annu. Rev. Phys. Chem.*, 2012, **63**, 541–569.
49 K. I. K. O. T. M. Satoshi Kaneco, *Energy Sources*, 2000, **22**, 127–135.
50 R. K. Yadav, J. O. Baeg, G. H. Oh, N. J. Park, K. J. Kong, J. Kim, D. W. Hwang and S. K. Biswas, *J. Am. Chem. Soc.*, 2012, **134**, 11455–11461.
51 D. Preti, S. Squarcialupi and G. Fachinetti, *Angew. Chem., Int. Ed.*, 2010, **49**, 2581–2584.
52 Z. Zhang, Y. Xie, W. Li, S. Hu, J. Song, T. Jiang and B. Han, *Angew. Chem., Int. Ed.*, 2008, **47**, 1127–1129.
53 Z. Zhang, S. Hu, J. Song, W. Li, G. Yang and B. Han, *ChemSusChem*, 2009, **2**, 234–238.
54 Y. Yasaka, C. Wakai, N. Matubayasi and M. Nakahara, *J. Phys. Chem. A*, 2010, **114**, 3510–3515.
55 S. Wesselbaum, U. Hintermair and W. Leitner, *Angew. Chem., Int. Ed.*, 2012, **51**, 8585–8588.

56 W. Leitner, *Nature*, 2000, **405**, 129–130.
57 S. N. Riduan, Y. Zhang and J. Y. Ying, *Angew. Chem., Int. Ed.*, 2009, **48**, 3322–3325.
58 G. Ménard and D. W. Stephan, *J. Am. Chem. Soc.*, 2010, **132**, 1796–1797.
59 A. E. Ashley, A. L. Thompson and D. O'Hare, *Angew. Chem., Int. Ed.*, 2009, **48**, 9839–9843.
60 B. Chan and L. Radom, *J. Am. Chem. Soc.*, 2006, **128**, 5322–5323.
61 B. Chan and L. Radom, *J. Am. Chem. Soc.*, 2008, **130**, 9790–9799.
62 S. Chakraborty, J. Zhang, J. A. Krause and H. Guan, *J. Am. Chem. Soc.*, 2010, **132**, 8872–8873.
63 J. Ma, N. N. Sun, X. L. Zhang, N. Zhao, F. K. Mao, W. Wei and Y. H. Sun, *Catal. Today*, 2009, **148**, 221–231.
64 F. Huang, G. Lu, L. Zhao, H. Li and Z.-X. Wang, *J. Am. Chem. Soc.*, 2010, **132**, 12388–12396.
65 G. Centi and S. Perathoner, *Catal. Today*, 2009, **148**, 191–205.
66 K. I. Tominaga, *Catal. Today*, 2006, **115**, 70–72.
67 B. Schäffner, F. Schäffner, S. P. Verevkin and A. Börner, *Chem. Rev.*, 2010, **110**, 4554–4581.
68 M. North, R. Pasquale and C. Young, *Green Chem.*, 2010, **12**, 1514–1539.
69 F. Jutz, J. M. Andanson and A. Baiker, *Chem. Rev.*, 2010, **111**, 322–353.
70 Z. Z. Yang, Y. N. Zhao and L. N. He, *RSC Adv.*, 2011, **1**, 545–567.
71 J. Zhang, J. Sun, X. Zhang, Y. Zhao and S. Zhang, *Greenhouse Gases: Sci. Technol.*, 2011, **1**, 142–159.
72 M. A. Pacheco and C. L. Marshall, *Energy Fuels*, 1997, **11**, 2–29.
73 J. Sun, L. Wang, S. Zhang, Z. Li, X. Zhang, W. Dai and R. Mori, *J. Mol. Catal. A: Chem.*, 2006, **256**, 295–300.
74 J. Sun, J. Ren, S. Zhang and W. Cheng, *Tetrahedron Lett.*, 2009, **50**, 423–426.
75 J. Q. Wang, J. Sun, W. G. Cheng, K. Dong, X. P. Zhang and S. J. Zhang, *Phys. Chem. Chem. Phys.*, 2012, **14**, 11021–11026.
76 J. Sun, S. Zhang, W. Cheng and J. Ren, *Tetrahedron Lett.*, 2008, **49**, 3588–3591.
77 J. Sun, L. Han, W. Cheng, J. Wang, X. Zhang and S. Zhang, *ChemSusChem*, 2011, **4**, 502–507.
78 Y. Zhou, S. Hu, X. Ma, S. Liang, T. Jiang and B. Han, *J. Mol. Catal. A: Chem.*, 2008, **284**, 52–57.
79 L. Han, S. J. Choi, M. S. Park, S. M. Lee, Y. J. Kim, M. I. Kim, B. Liu and D. W. Park, *React. Kinet., Mech. Catal.*, 2012, **106**, 25–35.
80 N. A. M. Razali, K. T. Lee, S. Bhatia and A. R. Mohamed, *Renewable Sustainable Energy Rev.*, 2012, **16**, 4951–4964.
81 W. L. Dai, S. L. Luo, S. F. Yin and C. T. Au, *Appl. Catal., A*, 2009, **366**, 2–12.
82 Z. F. Zhang, Z. W. Liu, J. Lu and Z. T. Liu, *Ind. Eng. Chem. Res.*, 2011, **50**, 1981–1988.
83 J. Du, J. Shi, Z. Li, Z. Liu, X. Fan and C. Tao, *J. Nat. Gas Chem.*, 2012, **21**, 476–479.
84 X. Chen, C. Hu, J. Su, T. Yu and Z. Gao, *Chin. J. Catal.*, 2006, **27**, 485–488.
85 L. Zhang, D. Niu, K. Zhang, G. Zhang, Y. Luo and J. Lu, *Green Chem.*, 2008, **10**, 202–206.
86 L. X. Wu, H. Wang, Y. Xiao, Z. Y. Tu, B. B. Ding and J. X. Lu, *Electrochem. Commun.*, 2012, **25**, 116–118.
87 X. Yuan, B. Lu, J. Liu, X. You, J. Zhao and Q. Cai, *J. Electrochem. Soc.*, 2012, **159**, E183–E186.
88 G. W. Huber, S. Iborra and A. Corma, *Chem. Rev.*, 2006, **106**, 4044–4098.
89 R. P. Swatloski, S. K. Spear, J. D. Holbrey and R. D. Rogers, *J. Am. Chem. Soc.*, 2002, **124**, 4974–4975.
90 A. Pinkert, K. N. Marsh, S. Pang and M. P. Staiger, *Chem. Rev.*, 2009, **109**, 6712–6728.
91 T. Vancov, A. S. Alston, T. Brown and S. McIntosh, *Renewable Energy*, 2012, **45**, 1–6.
92 C. Graenacher, *US Pat.*, 1943176, 1934.
93 C. Z. Liu, F. Wang, A. R. Stiles and C. Guo, *Appl. Energy*, 2012, **92**, 406–414.
94 T. Heinze, K. Schwikal and S. Barthel, *Macromol. Biosci.*, 2005, **5**, 520–525.
95 J. Wu, J. Zhang, H. Zhang, J. He, Q. Ren and M. Guo, *Biomacromolecules*, 2004, **5**, 266–268.
96 H. Zhang, J. Wu, J. Zhang and J. He, *Macromolecules*, 2005, **38**, 8272–8277.
97 K. Fukumoto, M. Yoshizawa and H. Ohno, *J. Am. Chem. Soc.*, 2005, **127**, 2398–2399.
98 Y. Fukaya, A. Sugimoto and H. Ohno, *Biomacromolecules*, 2006, **7**, 3295–3297.
99 Y. Fukaya, K. Hayashi, M. Wada and H. Ohno, *Green Chem.*, 2008, **10**, 44–46.
100 H. Zhao, G. A. Baker, Z. Song, O. Olubajo, T. Crittle and D. Peters, *Green Chem.*, 2008, **10**, 696–705.
101 A. S. Amarasekara and O. S. Owereh, *Ind. Eng. Chem. Res.*, 2009, **48**, 10152–10155.
102 A. Xu, J. Wang and H. Wang, *Green Chem.*, 2010, **12**, 268–275.
103 H. Wang, G. Gurau and R. D. Rogers, *Chem. Soc. Rev.*, 2012, **41**, 1519–1537.
104 R. Rinaldi, *Chem. Commun.*, 2011, **47**, 511–513.
105 P. Dominguez de Maria and A. Martinsson, *Analyst*, 2009, **134**, 493–496.
106 S. Köhler, T. Liebert and T. Heinze, *Macromol. Biosci.*, 2009, **9**, 836–841.
107 A. P. Abbott, T. J. Bell, S. Handa and B. Stoddart, *Green Chem.*, 2005, **7**, 705–707.
108 S. Possidonio, L. C. Fidale and O. A. El Seoud, *J. Polym. Sci., Part A: Polym. Chem.*, 2010, **48**, 134–143.
109 H. Ohno and Y. Fukaya, *Chem. Lett.*, 2009, **38**, 2–7.
110 N. Sun, H. Rodriguez, M. Rahman and R. D. Rogers, *Chem. Commun.*, 2011, **47**, 1405–1421.
111 J. Kahlen, K. Masuch and K. Leonhard, *Green Chem.*, 2010, **12**, 2172–2181.
112 R. C. Remsing, R. P. Swatloski, R. D. Rogers and G. Moyna, *Chem. Commun.*, 2006, 1271–1273.

113 R. C. Remsing, G. Hernandez, R. P. Swatloski, W. W. Massefski, R. D. Rogers and G. Moyna, *J. Phys. Chem. B*, 2008, **112**, 11071–11078.

114 T. G. A. Youngs, J. D. Holbrey, M. Deetlefs, M. Nieuwenhuyzen, M. F. C. Gomes and C. Hardacre, *ChemPhysChem*, 2006, **7**, 2279–2281.

115 G. Laus, G. Bentivoglio, H. Schottenberger, V. Kahlenberg, H. Kopacka, T. Röder and H. Sixta, *Lenzinger Ber.*, 2005, **84**, 71–85.

116 A. Shakeri and M. P. Staiger, *BioResources*, 2010, **5**, 979–989.

117 H. Olivier-Bourbigou, L. Magna and D. Morvan, *Appl. Catal., A*, 2010, **373**, 1–56.

118 T. Liebert and T. Heinze, *BioResources*, 2008, **3**, 576–601.

119 T. Erdmenger, C. Haensch, R. Hoogenboom and U. S. Schubert, *Macromol. Biosci.*, 2007, **7**, 440–445.

120 S. Barthel and T. Heinze, *Green Chem.*, 2006, **8**, 301–306.

121 T. G. A. Youngs, C. Hardacre and J. D. Holbrey, *J. Phys. Chem. B*, 2007, **111**, 13765–13774.

122 Y. L. Zhao, X. M. Liu, J. J. Wang and S. J. Zhang, *ChemPhysChem*, 2012, **13**, 3126–3133.

123 Y. Zhao, X. Liu, J. Wang and S. Zhang, *J. Phys. Chem. B*, 2013, **117**, 9042–9049.

124 Y. Zhao, X. Liu, J. Wang and S. Zhang, *Carbohydr. Polym.*, 2013, **94**, 723–730.

125 H. Liu, K. L. Sale, B. M. Holmes, B. A. Simmons and S. Singh, *J. Phys. Chem. B*, 2010, **114**, 4293–4301.

126 J. Zhang, H. Zhang, J. Wu, J. Zhang, J. He and J. Xiang, *Phys. Chem. Chem. Phys.*, 2010, **12**, 14829–14830.

127 J. Zhang, H. Zhang, J. Wu, J. Zhang, J. He and J. Xiang, *Phys. Chem. Chem. Phys.*, 2010, **12**, 1941–1947.

128 C. S. Lovell, A. Walker, R. A. Damion, A. Radhi, S. F. Tanner, T. Budtova and M. E. Ries, *Biomacromolecules*, 2010, **11**, 2927–2935.

129 J. Li, Y. Lu, D. Yang, Q. Sun, Y. Liu and H. Zhao, *Biomacromolecules*, 2011, **12**, 1860–1867.

130 A. Pinkert, K. N. Marsh and S. Pang, *Ind. Eng. Chem. Res.*, 2010, **49**, 11121–11130.

131 H. Zhao, C. L. Jones, G. A. Baker, S. Xia, O. Olubajo and V. N. Person, *J. Biotechnol.*, 2009, **139**, 47–54.

132 A. J. Ragauskas, C. K. Williams, B. H. Davison, G. Britovsek, J. Cairney, C. A. Eckert, W. J. Frederick, J. P. Hallett, D. J. Leak and C. L. Liotta, *Science*, 2006, **311**, 484–489.

133 Y. Q. Pu, N. Jiang and A. J. Ragauskas, *J. Wood Chem. Technol.*, 2007, **27**, 23–33.

134 V. B. Agbor, N. Cicek, R. Sparling, A. Berlin and D. B. Levin, *Biotechnol. Adv.*, 2011, **29**, 675–685.

135 Y. Sun and J. Cheng, *Bioresour. Technol.*, 2002, **83**, 1–11.

136 S. Tan and D. MacFarlane, in *Ionic Liquids*, ed. B. Kirchner, Springer Berlin Heidelberg, 2010, vol. 290, pp. 311–339.

137 A. Björkman, *Sven. Papperstidn.*, 1956, **59**, 477–485.

138 H. M. Chang, E. B. Cowling and W. Brown, *Holzforschung*, 1975, **29**, 153–159.

139 T. Ikeda, K. Holtman, J. F. Kadla, H.-m. Chang and H. Jameel, *J. Agric. Food Chem.*, 2002, **50**, 129–135.

140 B. J. Cox, S. Jia, Z. C. Zhang and J. G. Ekerdt, *Polym. Degrad. Stab.*, 2011, **96**, 426–431.

141 A. Casas, J. Palomar, M. V. Alonso, M. Oliet, S. Omar and F. Rodriguez, *Ind. Crops Prod.*, 2012, **37**, 155–163.

142 B. Li, J. Asikkala, I. Filpponen and D. S. Argyropoulos, *Ind. Eng. Chem. Res.*, 2010, **49**, 2477–2484.

143 D. Fu, G. Mazza and Y. Tamaki, *J. Agric. Food Chem.*, 2010, **58**, 2915–2922.

144 S. H. Lee, T. V. Doherty, R. J. Linhardt and J. S. Dordick, *Biotechnol. Bioeng.*, 2009, **102**, 1368–1376.

145 D. Robert, L. Perlack, A. Turhollow, R. Graham, B. Stokes, D. Erbach, *A joint study sponsored by US Department of Energy and US Department of Agriculture*, DOE/GO-102005-2135, ORNL/TM, 2005.

146 A. Brandt, J. Grasvik, J. P. Hallett and T. Welton, *Green Chem.*, 2013, **15**, 550–583.

147 J. Long, X. Li, L. Wang and N. Zhang, *Sci. China: Chem.*, 2012, **55**, 1500–1508.

148 I. Kilpelainen, H. Xie, A. King, M. Granstrom, S. Heikkinen and D. S. Argyropoulos, *J. Agric. Food Chem.*, 2007, **55**, 9142–9148.

149 N. Sun, M. Rahman, Y. Qin, M. L. Maxim, H. Rodriguez and R. D. Rogers, *Green Chem.*, 2009, **11**, 646–655.

150 N. Muhammad, Z. Man, M. A. Bustam, M. A. Mutalib, C. D. Wilfred and S. Rafiq, *Appl. Biochem. Biotechnol.*, 2011, **165**, 998–1009.

151 W. Y. Li, N. Sun, B. Stoner, X. Y. Jiang, X. M. Lu and R. D. Rogers, *Green Chem.*, 2011, **13**, 2038–2047.

152 C. Li, Q. Wang and Z. K. Zhao, *Green Chem.*, 2008, **10**, 177–182.

153 Q. Li, Y. C. He, M. Xian, G. Jun, X. Xu, J. M. Yang and L. Z. Li, *Bioresour. Technol.*, 2009, **100**, 3570–3575.

154 F. Hong, X. Guo, S. Zhang, S.-f. Han, G. Yang and L. J. Jonsson, *Bioresour. Technol.*, 2012, **104**, 503–508.

155 M. B. Turner, S. K. Spear, J. G. Huddleston, J. D. Holbrey and R. D. Rogers, *Green Chem.*, 2003, **5**, 443–447.

156 M. G. Adsul, A. P. Terwadkar, A. J. Varma and D. V. Gokhale, *BioResources*, 2009, **4**, 1670–1681.

157 M. S. Singhvi, M. G. Adsul and D. V. Gokhale, *Bioresour. Technol.*, 2011, **102**, 6569–6572.

158 N. Kamiya, Y. Matsushita, M. Hanaki, K. Nakashima, M. Narita, M. Goto and H. Takahashi, *Biotechnol. Lett.*, 2008, **30**, 1037–1040.

159 D. Antoni, V. V. Zverlov and W. H. Schwarz, *Appl. Microbiol. Biotechnol.*, 2007, **77**, 23–35.

160 P. Duerre, *Biotechnol. J.*, 2007, **2**, 1525–1534.

161 S. K. Lee, H. Chou, T. S. Ham, T. S. Lee and J. D. Keasling, *Curr. Opin. Biotechnol.*, 2008, **19**, 556–563.

162 L. M. Vane, *J. Chem. Technol. Biotechnol.*, 2005, **80**, 603–629.

163 P. Fatehi, *Biotechnol. Prog.*, 2013, **29**, 297–310.

164 G. Jurgens, S. Survase, O. Berezina, E. Sklavounos, J. Linnekoski, A. Kurkijarvi, M. Vakeva, A. van Heiningen and T. Granstrom, *Biotechnol. Lett.*, 2012, **34**, 1415–1434.

165 V. Menon and M. Rao, *Prog. Energy Combust. Sci.*, 2012, **38**, 522–550.

166 J. B. Binder and R. T. Raines, *J. Am. Chem. Soc.*, 2009, **131**, 1979–1985.

167 H. Zhao, J. E. Holladay, H. Brown and Z. C. Zhang, *Science*, 2007, **316**, 1597–1600.

168 C. Li, Z. Zhang and Z. K. Zhao, *Tetrahedron Lett.*, 2009, **50**, 5403–5405.

169 C. Shi, Y. Zhao, J. Xin, J. Wang, X. Lu, X. Zhang and S. Zhang, *Chem. Commun.*, 2012, **48**, 4103–4105.

170 M. Tan, L. Zhao and Y. Zhang, *Biomass Bioenergy*, 2011, **35**, 1367–1370.

171 X. Qi, M. Watanabe, T. M. Aida and R. L. Smith, Jr., *Cellulose*, 2011, **18**, 1327–1333.

172 B. Liu, Z. Zhang and Z. K. Zhao, *Chem. Eng. J.*, 2013, **215**, 517–521.

173 I. A. Ignatyev, C. Van Doorslaer, P. G. N. Mertens, K. Binnemans and D. E. de Vos, *ChemSusChem*, 2010, **3**, 91–96.

174 I. A. Ignatyev, C. V. Doorslaer, P. G. N. Mertens, K. Binnemans and D. E. de Vos, *Holzforschung*, 2011, **66**.

175 I. A. Ignatyev, P. G. N. Mertens, C. Van Doorslaer, K. Binnemans and D. E. de Vos, *Green Chem.*, 2010, **12**, 1790–1795.

176 Z. Zhang and Z. K. Zhao, *Bioresour. Technol.*, 2010, **101**, 1111–1114.

177 K. R. Enslow and A. T. Bell, *RSC Adv.*, 2012, **2**, 10028–10036.

178 L. Zhang, H. Yu, P. Wang, H. Dong and X. Peng, *Bioresour. Technol.*, 2013, **130**, 110–116.

179 L. Vanoye, L. M. Fanselow, J. D. Holbrey, M. P. Atkins and K. R. Seddon, *Green Chem.*, 2009, **11**, 390–396.

180 J. B. Binder, M. J. Gray, J. F. White, Z. C. Zhang and J. E. Holladay, *Biomass Bioenergy*, 2009, **33**, 1122–1130.

181 S. Jia, B. J. Cox, X. Guo, Z. C. Zhang and J. G. Ekerdt, *ChemSusChem*, 2010, **3**, 1078–1084.

182 S. Jia, B. J. Cox, X. Guo, Z. C. Zhang and J. G. Ekerdt, *Ind. Eng. Chem. Res.*, 2011, **50**, 849–855.

183 M. M. Hossain and L. Aldous, *Aust. J. Chem.*, 2012, **65**, 1465–1477.

184 A. Chen, E. I. Rogers and R. G. Compton, *Electroanalysis*, 2010, **22**, 1037–1044.

185 E. Reichert, R. Wintringer, D. A. Volmer and R. Hempelmann, *Phys. Chem. Chem. Phys.*, 2012, **14**, 5214–5221.

186 B. O'Regan and M. Grätzel, *Nature*, 1991, **353**, 737–740.

187 A. Yella, H. W. Lee, H. N. Tsao, C. Yi, A. K. Chandiran, M. K. Nazeeruddin, E. W. Diau, C. Y. Yeh, S. M. Zakeeruddin and M. Grätzel, *Science*, 2011, **334**, 629–634.

188 M. K. Nazeeruddin, F. De Angelis, S. Fantacci, A. Selloni, G. Viscardi, P. Liska, S. Ito, B. Takeru and M. Grätzel, *J. Am. Chem. Soc.*, 2005, **127**, 16835–16847.

189 M. Gorlov and L. Kloo, *Dalton Trans.*, 2008, 2655–2666.

190 S. M. Zakeeruddin and M. Grätzel, *Adv. Funct. Mater.*, 2009, **19**, 2187–2202.

191 N. Papageorgiou, Y. Athanassov, M. Armand, P. Bonhote, H. Pettersson, A. Azam and M. Grätzel, *J. Electrochem. Soc.*, 1996, **143**, 3099–3108.

192 P. Wang, S. M. Zakeeruddin, J.-E. Moser and M. Grätzel, *J. Phys. Chem. B*, 2003, **107**, 13280–13285.

193 P. Wang, S. M. Zakeeruddin, R. Humphry-Baker and M. Grätzel, *Chem. Mater.*, 2004, **16**, 2694–2696.

194 P. Wang, B. Wenger, R. Humphry-Baker, J.-E. Moser, J. Teuscher, W. Kantlehner, J. Mezger, E. V. Stoyanov, S. M. Zakeeruddin and M. Grätzel, *J. Am. Chem. Soc.*, 2005, **127**, 6850–6856.

195 Y. Bai, Y. Cao, J. Zhang, M. Wang, R. Li, P. Wang, S. M. Zakeeruddin and M. Grätzel, *Nat. Mater.*, 2008, **7**, 626–630.

196 D. Shi, N. Pootrakulchote, R. Li, J. Guo, Y. Wang, S. M. Zakeeruddin, M. Grätzel and P. Wang, *J. Phys. Chem. C*, 2008, **112**, 17046–17050.

197 D. Kuang, S. Uchida, R. Humphry-Baker, S. M. Zakeeruddin and M. Gratzel, *Angew. Chem., Int. Ed.*, 2008, **47**, 1923–1927.

198 D. Kuang, P. Comte, S. M. Zakeeruddin, D. P. Hagberg, K. M. Karlsson, L. Sun, M. K. Nazeeruddin and M. Grätzel, *Sol. Energy*, 2011, **85**, 1189–1194.

199 M. Xu, S. Wenger, H. Bala, D. Shi, R. Li, Y. Zhou, S. M. Zakeeruddin, M. Grätzel and P. Wang, *J. Phys. Chem. C*, 2009, **113**, 2966–2973.

200 H. Santa-Nokki, S. Busi, J. Kallioinen, M. Lahtinen and J. Korppi-Tommola, *J. Photochem. Photobiol., A*, 2007, **186**, 29–33.

201 N. Cai, J. Zhang, D. Zhou, Z. Yi, J. Guo and P. Wang, *J. Phys. Chem. C*, 2009, **113**, 4215–4221.

202 L. Guo, X. Pan, M. Wang, C. Zhang, X. Fang, S. Chen and S. Dai, *Sol. Energy*, 2011, **85**, 7–11.

203 L. Guo, X. Pan, C. Zhang, W. Liu, M. Wang, X. Fang and S. Dai, *Sol. Energy*, 2010, **84**, 373–378.

204 Q. Miao, S. Zhang, H. Xu, P. Zhang and H. Li, *Chem. Commun.*, 2013, **49**, 6980–6982.

205 J. Zhao, F. Yan, L. Qiu, Y. Zhang, X. Chen and B. Sun, *Chem. Commun.*, 2011, **47**, 11516–11518.

206 L. Wang, H. Zhang, R. Ge, C. Wang, W. Guo, Y. Shi, Y. Gao and T. Ma, *RSC Adv.*, 2013, **3**, 12975–12980.

207 P. Wang, S. M. Zakeeruddin, J.-E. Moser, R. Humphry-Baker and M. Grätzel, *J. Am. Chem. Soc.*, 2004, **126**, 7164–7165.

208 H. Tian, Z. Yu, A. Hagfeldt, L. Kloo and L. Sun, *J. Am. Chem. Soc.*, 2011, **133**, 9413–9422.

209 H. Tian, E. Gabrielsson, Z. Yu, A. Hagfeldt, L. Kloo and L. Sun, *Chem. Commun.*, 2011, **47**, 10124–10126.

210 P. Wang, S. M. Zakeeruddin, P. Comte, I. Exnar and M. Grätzel, *J. Am. Chem. Soc.*, 2003, **125**, 1166–1167.

211 P. Cheng, T. Lan, W. Wang, H. Wu, H. Yang, C. Deng, X. Dai and S. Guo, *Sol. Energy*, 2010, **84**, 854–859.

212 P. Y. Chen, C. P. Lee, R. Vittal and K. C. Ho, *J. Power Sources*, 2010, **195**, 3933–3938.

213 L. Jin, Z. Wu, T. Wei, J. Zhai and X. Zhang, *Chem. Commun.*, 2011, **47**, 997–999.

214 L. Wang, S. Fang, Y. Lin, X. Zhou and M. Li, *Chem. Commun.*, 2005, 5687–5689.

215 M. Wang, X. Yin, X. R. Xiao, X. Zhou, Z. Z. Yang, X. P. Li and Y. Lin, *J. Photochem. Photobiol., A*, 2008, **194**, 20–26.

216 S. Sun, J. Song, R. Feng and Z. Shan, *Electrochim. Acta*, 2012, **69**, 51–55.

217 D. Qin, Y. Zhang, S. Huang, Y. Luo, D. Li and Q. Meng, *Electrochim. Acta*, 2011, **56**, 8680–8687.

218 Y. Fang, W. Xiang, X. Zhou, Y. Lin and S. Fang, *Electrochem. Commun.*, 2011, **13**, 60–63.

219 J. Zhao, X. Shen, F. Yan, L. Qiu, S. Lee and B. Sun, *J. Mater. Chem.*, 2011, **21**, 7326–7330.

220 X. Chen, Q. Li, J. Zhao, L. Qiu, Y. Zhang, B. Sun and F. Yan, *J. Power Sources*, 2012, **207**, 216–221.

221 J. Shi, L. Wang, Y. Liang, S. Peng, F. Cheng and J. Chen, *J. Phys. Chem. C*, 2010, **114**, 6814–6821.

222 C. P. Lee, L. Y. Lin, P. Y. Chen, R. Vittal and K. C. Ho, *J. Mater. Chem.*, 2010, **20**, 3619–3625.

223 B. X. Lei, W. J. Fang, Y. F. Hou, J. Y. Liao, D. B. Kuang and C. Y. Su, *J. Photochem. Photobiol., A*, 2010, **216**, 8–14.

224 R. Kawano, T. Katakabe, H. Shimosawa, M. K. Nazeeruddin, M. Grätzel, H. Matsui, T. Kitamura, N. Tanabe and M. Watanabe, *Phys. Chem. Chem. Phys.*, 2010, **12**, 1916–1921.

225 W. S. Chi, J. K. Koh, S. H. Ahn, J.-S. Shin, H. Ahn, D. Y. Ryu and J. H. Kim, *Electrochem. Commun.*, 2011, **13**, 1349–1352.

226 S. H. Ahn, W. S. Chi, J. T. Park, J. K. Koh, D. K. Roh and J. H. Kim, *Adv. Mater.*, 2012, **24**, 519–522.

227 G. Wang, L. Wang, S. Zhuo, S. Fang and Y. Lin, *Chem. Commun.*, 2011, **47**, 2700–2702.

228 A. Midya, Z. Xie, J. X. Yang, Z. K. Chen, D. J. Blackwood, J. Wang, S. Adams and K. P. Loh, *Chem. Commun.*, 2010, **46**, 2091–2093.

229 H. Wang, X. Zhang, F. Gong, G. Zhou and Z. S. Wang, *Adv. Mater.*, 2012, **24**, 121–124.

230 V. Armel, M. Forsyth, D. R. MacFarlane and J. M. Pringle, *Energy Environ. Sci.*, 2011, **4**, 2234–2239.

231 Q. Li, J. Zhao, B. Sun, B. Lin, L. Qiu, Y. Zhang, X. Chen, J. Lu and F. Yan, *Adv. Mater.*, 2012, **24**, 945–950.

232 T. Sugimoto, Y. Atsumi, M. Kono, M. Kikuta, E. Ishiko, M. Yamagata and M. Ishikawa, *J. Power Sources*, 2010, **195**, 6153–6156.

233 X. G. Sun, C. Liao, N. Shao, J. R. Bell, B. Guo, H. Luo, D. E. Jiang and S. Dai, *J. Power Sources*, 2013, **237**, 5–12.

234 H. Usui, Y. Yamamoto, K. Yoshiyama, T. Itoh and H. Sakaguchi, *J. Power Sources*, 2011, **196**, 3911–3915.

235 H. Usui, M. Shimizu and H. Sakaguchi, *J. Power Sources*, 2013, **235**, 29–35.

236 G. Kim, S. Jeong, M. Joost, E. Rocca, M. Winter, S. Passerini and A. Balducci, *J. Power Sources*, 2011, **196**, 2187–2194.

237 M. Nádherná, J. Reiter, J. Moškon and R. Dominko, *J. Power Sources*, 2011, **196**, 7700–7706.

238 J. Y. Huang, L. Zhong, C. M. Wang, J. P. Sullivan, W. Xu, L. Q. Zhang, S. X. Mao, N. S. Hudak, X. H. Liu and A. Subramanian, *Science*, 2010, **330**, 1515–1520.

239 M. Patel, M. Gnanavel and A. J. Bhattacharyya, *J. Mater. Chem.*, 2011, **21**, 17419–17424.

240 H. Kim, Y. Ding and P. A. Kohl, *J. Power Sources*, 2012, **198**, 281–286.

241 A. Senda, K. Matsumoto, T. Nohira and R. Hagiwara, *J. Power Sources*, 2010, **195**, 4414–4417.

242 L. Siinor, K. Lust and E. Lust, *Electrochem. Commun.*, 2010, **12**, 1058–1061.

243 C. Liu, Z. Yu, D. Neff, A. Zhamu and B. Z. Jang, *Nano Lett.*, 2010, **10**, 4863–4868.

244 L. Wei, M. Sevilla, A. B. Fuertes, R. Mokaya and G. Yushin, *Adv. Funct. Mater.*, 2012, **22**, 827–834.

245 L. Timperman, H. Galiano, D. Lemordant and M. Anouti, *Electrochem. Commun.*, 2011, **13**, 1112–1115.

246 T. Y. Kim, H. W. Lee, M. Stoller, D. R. Dreyer, C. W. Bielawski, R. S. Ruoff and K. S. Suh, *ACS Nano*, 2011, **5**, 436–442.

247 Y. Shim and H. J. Kim, *ACS Nano*, 2010, **4**, 2345–2355.

248 Y. J. Kang, H. Chung, C.-H. Han and W. Kim, *Nanotechnology*, 2012, **23**, 065401.

249 Y. J. Kang, S. J. Chun, S. S. Lee, B. Y. Kim, J. H. Kim, H. Chung, S. Y. Lee and W. Kim, *ACS Nano*, 2012, **6**, 6400–6406.

250 G. Pandey and S. Hashmi, *J. Mater. Chem. A*, 2013, **1**, 3372–3378.

251 M. R. M. Anouti, L. Timperman, M. el Hilali, A. L. Boisset and H. Galiano, *J. Phys. Chem. C*, 2012, **116**, 9412–9418.

252 T. Zhang and H. Zhou, *Angew. Chem., Int. Ed.*, 2012, **51**, 11062–11067.

253 D. Zhang, R. Li, T. Huang and A. Yu, *J. Power Sources*, 2010, **195**, 1202–1206.

254 Z. Guo, G. Zhu, Z. Qiu, Y. Wang and Y. Xia, *Electrochem. Commun.*, 2012, **25**, 26–29.

255 Q. Luo, L. Li, W. Wang, Z. Nie, X. Wei, B. Li, B. Chen, Z. Yang and V. Sprenkle, *ChemSusChem*, 2013, **6**, 268–274.

256 W. Wang, Q. Luo, B. Li, X. Wei, L. Li and Z. Yang, *Adv. Funct. Mater.*, 2012, **23**, 970–986.

257 D. Zhang, Q. Liu, X. Shi and Y. Li, *J. Power Sources*, 2012, **203**, 201–205.